Sedimentary Geology 421 (2021) 105954

Contents lists available at ScienceDirect

Sedimentary Geology

journal homepage: www.elsevier.com/locate/sedgeo

Milankovitch cyclicity in the latest Cretaceous of the Gulf Coastal Plain, USA

Jonė Naujokaitytė [a,d,*], Matthew P. Garb [a], Nicolas Thibault [b], Shannon K. Brophy [a,f], Neil H. Landman [c], James D. Witts [e], J. Kirk Cochran [d], Ekaterina Larina [f], George Phillips [g], Corinne E. Myers [e]

[a] CUNY Brooklyn College, Department of Earth and Environmental Science, Brooklyn, NY 11210, USA
[b] Department of Geosciences and Natural Resource Management, University of Copenhagen, Øster Voldgade 10, DK-1350 Copenhagen, Denmark
[c] American Museum of Natural History, Division of Paleontology (Invertebrates), New York 10024, USA
[d] University of New Mexico, Department of Earth and Planetary Sciences, Albuquerque, NM 87131, USA
[e] School of Marine and Atmospheric Sciences, Stony Brook University, Stony Brook, NY 11794, USA
[f] University of Southern California, Department of Earth Sciences, Los Angeles, CA 90018, USA
[g] Mississippi Museum of Natural Science, Division of Paleontology, Jackson, MS 39202, USA

ARTICLE INFO

Article history:
Received 19 March 2021
Received in revised form 29 May 2021
Accepted 29 May 2021
Available online 11 June 2021

Editor: Dr. Brian Jones

Keywords:
K–Pg mass extinction
Cyclostratigraphy
Stable isotopes
Orbital cycles
Chemostratigraphy

ABSTRACT

Upper Cretaceous marine sequences in the Gulf Coastal Plain (USA) span the Cretaceous–Paleogene (K–Pg) transition, allowing for detailed studies of one of the most severe extinction events of the Phanerozoic. To improve the temporal resolution of the stratigraphic record that represents environmental change leading up to the K–Pg boundary, we constructed a high-resolution chemostratigraphy and cyclostratigraphy of upper Maastrichtian shallow marine deposits located in the state of Mississippi (USA). Upper Maastrichtian strata in this area consist of alternating decimeter scale chalk and marl rhythmites deposited in a hemipelagic setting. New geochemical proxy records were used to test whether rhythmic sedimentation was driven by Milankovitch cycles. Stable isotopes ($\delta^{13}C_{carb}$, $\delta^{18}O_{carb}$), carbonate content (wt% $CaCO_3$), and elemental concentrations (Ti, K, Fe) integrated with microfossil and ammonite biostratigraphy reveal astronomical forcing in the studied record. Spectral estimation suggests that rhythmic bedding was associated with climate change driven by precession (~20 kyr). Obliquity signals are also apparent in our analysis, and short eccentricity (~100 kyr) is inferred from amplitude modulation of precession. Studied sections were correlated at the precession scale with the recently tuned K–Pg succession near Morello, Italy which is stratigraphically equivalent to the well-characterized K–Pg sites in Gubbio, Italy (Bottaccione, Contessa Highway). Additionally, carbon isotope records from the study area exhibit large scale trends throughout the latest Maastrichtian, similar to those observed in the Morello and Bottaccione sections. Thus, we show that Milankovitch-scale climatic signals and low-amplitude carbon isotope shifts (<0.5‰) of the late Maastrichtian of the Gulf Coastal Plain are well-preserved and can be correlated globally.

1. Introduction

The Late Cretaceous is characterized by several global-scale disturbances, including the Cretaceous–Paleogene (K–Pg) mass extinction (e.g. Bralower, 2002; Batenburg et al., 2017; Gilleaudeau et al., 2018; Barnet et al., 2019). Ample evidence suggests that extremely rapid environmental change associated with the Chicxulub bolide impact was the principal cause of the K–Pg extinction (e.g., Alvarez et al., 1980; Schulte et al., 2010; Hull et al., 2020; Chiarenza et al., 2020). Studies of K–Pg boundary sites from around the globe indicate that impact ejecta deposits coincide with a severe biotic collapse at the boundary (Schulte et al., 2010; Hull et al., 2020). Global-scale perturbations following the impact may have occurred due to vaporization of sulfur-rich carbonate target rock, with important 'kill mechanisms' likely including an impact winter, disruption of sunlight and photosynthesis, widespread wildfires, and acid rain leading to transient ocean acidification (e.g., Sheehan and Hansen, 1986; Vellekoop et al., 2014; Vellekoop et al., 2016; Henehan et al., 2019; Alvarez et al., 2019).

Other studies propose a more gradual extinction associated with climate warming and environmental changes induced by emplacement of the Deccan Trap Large Igneous Province (LIP) in India (Keller, 2005; Punekar et al., 2016; Keller et al., 2020). This LIP erupted over a <1-million-year period during the latest Cretaceous and early Paleogene, essentially spanning the Chicxulub impact and mass extinction (Schoene et al., 2019; Sprain et al., 2019; Eddy et al., 2020). A potential link between Deccan volcanism and the K–Pg extinction is therefore of

* Corresponding author at: University of New Mexico, Department of Earth and Planetary Sciences, Albuquerque, NM 87131, USA.
E-mail address: jnaujokaityte@unm.edu (J. Naujokaitytė).

https://doi.org/10.1016/j.sedgeo.2021.105954
0037-0738/

interest, as several older mass extinction events have been attributed to the environmental effects of LIP eruptions, including those at the Permian–Triassic (P–T) and Triassic–Jurassic (T–J) boundaries (e.g., Wignall, 2001; Saunders, 2005; Barnosky et al., 2011; Bond and Wignall, 2014; Tegner et al., 2020). Debate persists regarding the exact role of the Deccan Traps in the K–Pg extinction, which is partially due to poor temporal resolution of geochemical proxy records (Schoene et al., 2019; Sprain et al., 2019; Hull et al., 2020). Thus, additional insights may be gained by linking K–Pg records to higher-resolution Milankovitch-scale environmental change in the late Maastrichtian.

The Gulf Coastal Plain (GCP; Fig. 1A, B) region of the USA has undergone extensive investigation of the K–Pg transition. Abundant exposures of marine K–Pg sequences have resulted in numerous paleontological and stratigraphic studies that provide essential information on late Maastrichtian marine conditions, the effects of the Chicxulub bolide impact, and recovery during the early Danian (e.g., Mancini, 1996; Smit et al., 1996; Schulte et al., 2010; Hart et al., 2014; Larina et al., 2016; Witts et al., 2018; Alvarez et al., 2019; Witts et al., 2021). However, high-resolution chemostratigraphy has not been established for the late Maastrichtian in the GCP. Here, we present new chemostratigraphic ($\delta^{13}C_{carb}$, $\delta^{18}O_{carb}$, wt%$CaCO_3$, and elemental concentrations) data from two uppermost Maastrichtian sequences located in Mississippi (American Museum of Natural History (AMNH) locality #3525, AMNH locality #3483; Fig. 1B). Cyclical changes in lithology and independent biostratigraphic constraints facilitate recognition of orbital cycles in the latest Cretaceous Prairie Bluff Chalk (PBC). Here, we use new chemostratigraphic data to 1) ascertain the presence of Milankovitch cycles in the GCP sections; 2) correlate GCP sections

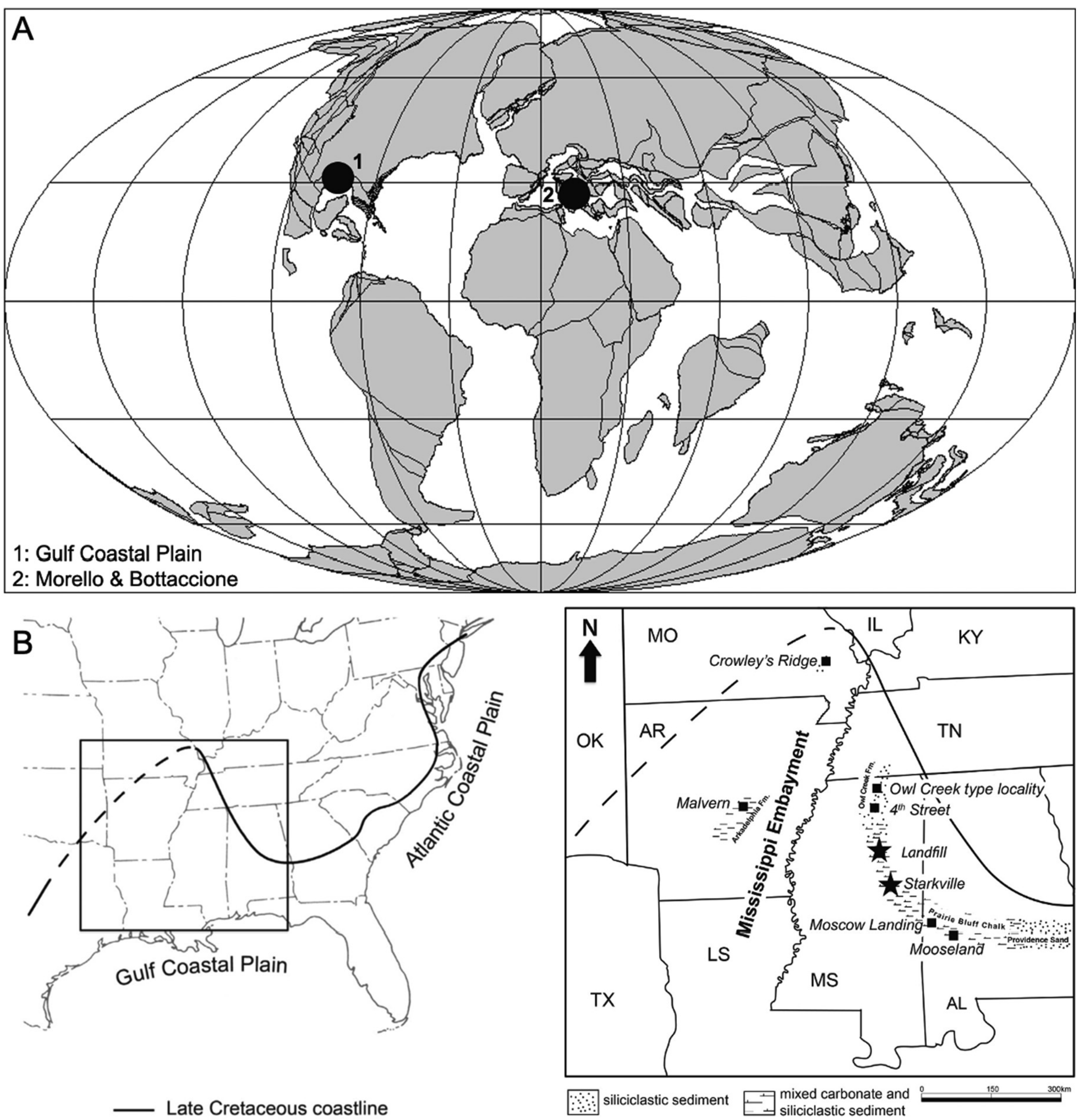

Fig. 1. A: Late Cretaceous paleogeography. Reconstruction modified from http://www.serg.unicam.it/Reconstructions.htm (Schettino and Scotese, 2005). The GCP study area (1) and the Bottaccione and Morello localities (2) are indicated by black circles. B: (Left) Map of southeastern Unites States showing the study area and the Late Cretaceous paleoshoreline. (Right) Close-up of the Cretaceous outcrop belt and location of study sites (indicated by black stars). The black squares indicate other localities from the biostratigraphic study conducted by Larina et al. (2016), on which we base our study.
Image modified from Larina et al. (2016).

with pelagic carbonates of the Umbria–Marche basin in Morello, Italy using $\delta^{13}C_{carb}$ and pXRF data obtained from Sinnesael et al. (2016, 2018); and 3) provide age estimates for the GCP sections based on cyclostratigraphic correlation with the Morello section (calibrated in terms of magneto- and cyclostratigraphy), which have a known relationship with the type section of the K–Pg extinction in Gubbio, Italy (Alvarez et al., 1980). Our results indicate the presence of Milankovitch cycles (precession, obliquity and short eccentricity) in most proxy data, providing a foundation for constructing a late Maastrichtian astronomical timescale for this region, an invaluable tool for future paleoenvironmental studies of the GCP. We use our cyclostratigraphic framework to correlate GCP carbon isotope records to published $\delta^{13}C$ data obtained from pelagic carbonates of the Umbria–Marche basin, Italy. Similar trends and distinctive small-amplitude shifts in $\delta^{13}C$ data indicate a potential global-scale carbon isotope signal in GCP strata. Additionally, we investigate calcareous nannofossil records to constrain the biostratigraphy of our study area and to obtain a more comprehensive understanding of local environmental change during the latest Cretaceous.

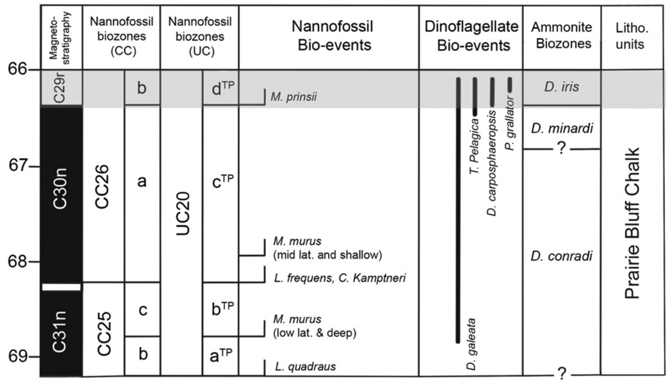

Fig. 2. Maastrichtian biostratigraphy and magnetostratigraphy for the Prairie Bluff Chalk in the Gulf Coastal Plain. Image modified from Larina et al. (2016). The timeframe in this study is highlighted in light gray. Magnetostratigraphy is based on correlation and was not measured for the PBC. From left to right: Magnetochrons, CC and UC calcareous nannofossil biozones and first occurrences in the GCP; dinoflagellate and ammonite biostratigraphy; lithostratigrahpic units (litho units; Prairie Bluff Chalk).

2. Geologic setting

2.1. The Mississippi Embayment

The study area is located in the Gulf Coastal Plain (GCP) of the United States within the eastern margin of the Mississippi Embayment (Fig. 1). During the Late Cretaceous, the region was inundated by a shallow sea that extended from present-day Louisiana to southernmost Illinois (Fig. 1B; Pryor, 1960; Dastas et al., 2014; Larina et al., 2016). Deposition was dominated by coastal and shallow marine processes resulting in mixed carbonate–siliciclastic successions (Mancini, 1996; Cox and Van Arsdale, 2002). Upper Cretaceous units occur within an outcrop belt that extends from the eastern to the western margin of the Mississippi Embayment (Fig. 1B; Liu, 2009). In the study area, the Prairie Bluff Chalk (PBC) records an offshore, outer neritic environment deposited on a broad, shallow shelf ~50–100 m deep (Zachos et al., 1989). The PBC is overlain by the Clayton Formation (Clayton Fm) of Danian age. The contact between the PBC and the Clayton Fm marks the K–Pg boundary. In some areas of this region, the basal Clayton Fm is a spherule-rich sand unit which may represent mass transport or tsunamite deposits related to the Chicxulub impact (Smit et al., 1996; Witts et al., 2018). Other sites exhibit a heavily bioturbated K–Pg contact overlain by silty marls of the Danian age Clayton Fm.

2.2. Biostratigraphy

Paleomagnetic and radio-isotopic constraints have yet to be established for the studied sections. Thus, we use a combination of new and existing biostratigraphic data to constrain our geochemical analyses. Biozonation schemes based on planktonic foraminifera, calcareous nannofossils and ammonites have been established for Upper Cretaceous sequences in the study region (Fig. 2; Mancini et al., 1989; Puckett, 2005; Larina et al., 2016). Mancini et al. (1989) assigned the PBC to the middle late Maastrichtian *Globotruncana aegyptiaca* and *Racemiguembelina fructicosa* planktonic foraminiferal biozones. The absence of several latest Maastrichtian foraminifera (e.g., *Abathomphalus mayaroensis*) has been attributed to ecological preference of this taxon for deep water and higher latitude environments rather than representing a significant sedimentary gap (Nifuku et al., 2009; Larina et al., 2016). The uppermost Maastrichtian planktonic foraminifer *Plummerita hantkeninoides* (CF1 Zone) has not been recovered from the PBC, but has been found in stratigraphically equivalent, deeper water sites in the GCP (Brazos River, TX), supporting that the absence of late Maastrichtian planktonic foraminifera is more likely due to environmental preferences than a depositional hiatus (Abramovich et al., 2011; Witts et al., 2021). Despite the absence of upper Maastrichtian foraminifera, the presence of calcareous nannofossil, dinoflagellate and macroinvertebrate biostratigraphic markers suggest a latest Maastrichtian timeframe for the PBC (Larina et al., 2016).

A high-resolution ammonite biozonation for the GCP was constructed by Larina et al. (2016). Three upper Maastrichtian biozones were established based on correlation with records from the Atlantic Coastal Plain (Landman et al., 2004; Landman et al., 2007). The oldest biozone is represented by the scaphitid ammonite *Discoscaphites conradi*, followed by the *D. minardi* Zone and the youngest *D. iris* Zone (Fig. 2). Larina et al. (2016) integrated the ammonite biostratigraphy of the GCP with calcareous nannofossil zones and dinoflagellate biostratigraphy. The base of the *D. conradi* biozone occurs within nannofossil subzone CC25b/UC20a^{TP} defined by the first occurrence (FO) of *Lithraphidites quadratus*. In the GCP, the upper part of subzones CC25b and UC20a^{TP} are correlative to the upper boundary of dinoflagellate marker *Isabelidinium cooksoniae* and the lower boundary of dinoflagellate *Deflandrea galeata* (Edwards et al., 1999; Larina et al., 2016). The *D. conradi* zone extends to the top of CC26a/UC20c^{TP}, defined by the occurrence of calcareous nannofossil *Micula murus*. The *D. minardi* biozone lies within subzones CC26a and UC20c^{TP}. The base of the *D. iris* biozone is correlative with the FO of *Palynodinium grallator*, an uppermost Maastrichtian dinoflagellate marker (e.g. Firth, 1987; FitzPatrick et al., 2018) and the base of subzones CC26b/UC20d^{TP}, marked by the FO of calcareous nannofossil *Micula prinsii*, representing the uppermost Maastrichtian (Fig. 2; Thibault et al., 2012; Gardin et al., 2012; Larina et al., 2016). The occurrence of latest Maastrichtian nannofossil, dinoflagellate and ammonite biostratigraphic markers therefore indicates a relatively complete late Maastrichtian record in the GCP.

3. Study area

3.1. Starkville, Oktibbeha County, Mississippi (AMNH locality #3525)

The sampled section at Starkville consists of 7.9 m of the PBC overlain by 0.3 m of the Clayton Fm (Fig. 1B). The PBC is composed of decimeter scale (~0.3–0.4 m), heavily bioturbated, slightly micaceous, silty marls alternating with indurated, gray to white, slightly micaceous, bioturbated chalks. Chalk and marl couplets are ~50–60 cm thick (Fig. 3B) and generally, the silty marl horizons are thicker than the chalks. Burrows infilled with the lithology of overlying strata are observed throughout the section, indicating that chalk and marl couplets are of primary origin as opposed to an artifact of differential diagenesis (Westphal et al., 2010). The carbonate fraction of the PBC mainly

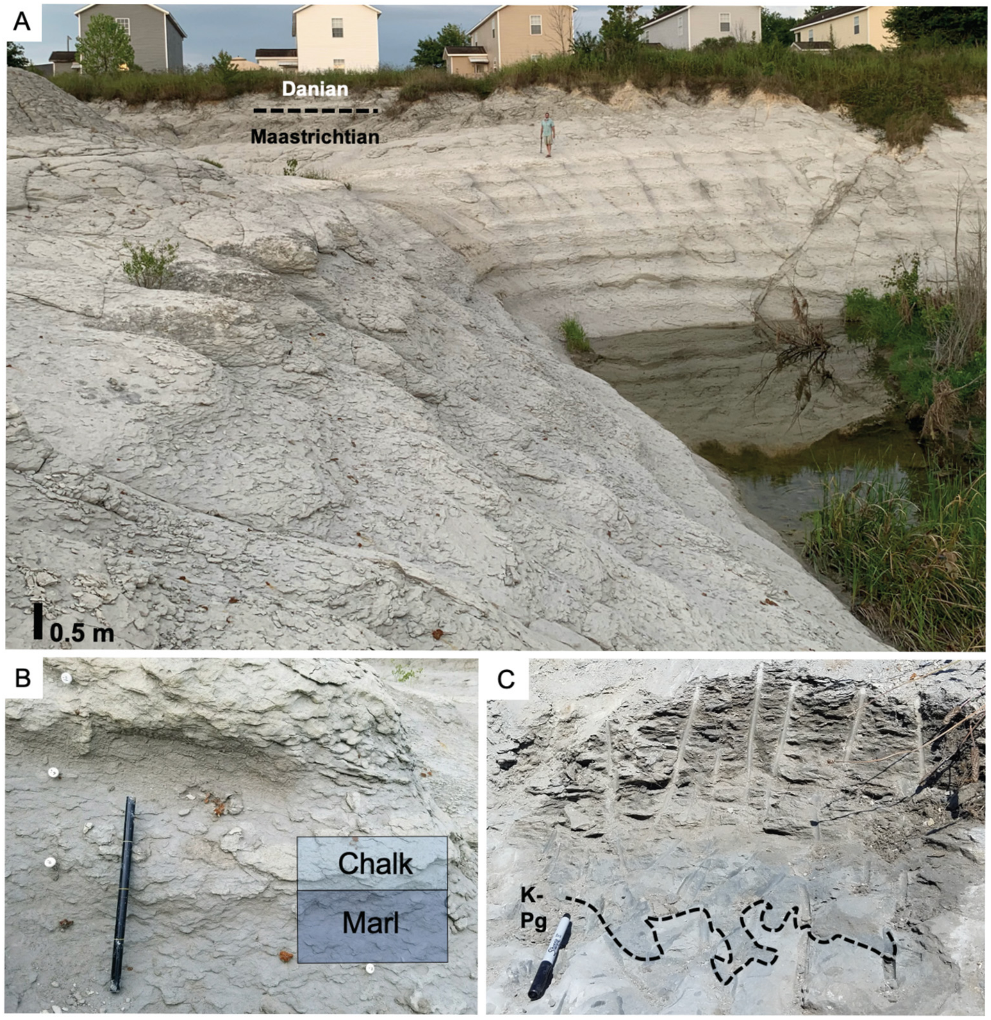

Fig. 3. Starkville, Mississippi locality A: Overview of the Starkville section. The K–Pg boundary is marked in dashed black B: A chalk–marl couplet highlighted in light (chalk) and dark (marl) blue. White pins mark 20 cm intervals. C: Close-up of the K–Pg boundary (outlined in dashed black) characterized by *Thalassinoides* trace fossils indicated by Clayton Fm. sediment (dark gray) piping down into the Prairie Bluff Chalk. (For interpretation of the references to color in this figure legend, the reader is referred to the web version of this article.)

consists of well-preserved calcareous nannofossils and some foraminifera. The top 3.5 m of the PBC is rich in mollusks preserved as internal molds, including *Discoscaphites iris*. In contrast, the basal 4.4 m of the section is characterized by a sparse molluskan fauna, primarily composed of oysters and pectinid bivalves. The transition from the PBC to the Clayton Fm spans the K–Pg boundary. This unconformable boundary is undulating and heavily bioturbated with *Thalassinoides* burrows piping down Clayton Fm sediments into the PBC. Here, the Clayton Fm is a 0.3 m thick, silty, micaceous and marly fine sand.

At Starkville, *Discoscaphites iris* is abundant in the upper ~3.5 m of the PBC (Fig. 5A). Due to a lack of preserved macroinvertebrates in the basal ~4.4 m, the first occurrence of *D. iris* is not accurately constrained in this section. Larina et al. (2016) suggest that the *D. iris* Zone extends to ~8 m below the K–Pg boundary based on the lowest occurrence of the dinoflagellate *Palynodinium grallator* at this level. Several ammonite species from the *D. iris* assemblage zone occur at the top of the section, including *Eubaculites carinatus* and *E. latecarinatus* (Landman et al., 2004; Landman et al., 2007; Witts et al., 2021). Existing calcareous nannofossil data from Starkville is low-resolution, with few age-diagnostic taxa present (Larina et al., 2016). To obtain a more accurate biozonation and better constrain geochemical data, eight new samples were analyzed for calcareous nannofossils (see Results section).

3.2. Prairie Bluff (PB) Landfill, Chickasaw County, Mississippi (AMNH locality)

The sampled section at the PB Landfill is 6.5 m thick (Figs. 4A, 6A). Rhythmic bedding is apparent but thicker and less prominent than at Starkville (Figs. 4, 6). Each rhythmite is up to ~1 m thick, as opposed to ~0.5–0.6 m at Starkville. Here, the PBC consists of gray, highly bioturbated, slightly micaceous silty marls alternating with light gray, massive, bioturbated, slightly micaceous chalks. Generally, the Landfill section is more fossiliferous than Starkville, with gastropods, bivalves, ammonites, and shark teeth scattered throughout the section. The PBC–Clayton Fm contact is sharp and marks the K–Pg boundary (Fig. 4C). The basal Clayton Fm is characterized by a ~2.5 m thick, cross-bedded, coarse grained, quartz sand unit.

Based on Larina et al. (2016) biostratigraphic study, the PB Landfill locality spans the *D. minardi* and *D. iris* ammonite biozones. The lowest occurrence of *D. minardi* is documented 13 m below the K–Pg, and the lowest occurrence of *D. iris* is documented 9 m below the K–Pg. Ammonite taxa associated with the *D. minardi* and *D. iris* biozones occur throughout the section and include *Trachyscaphites alabamensis*, *Eubaculites carinatus*, *E. latecarinatus* and *E. labyrinthicus* (Figs. 4, 6; Larina et al., 2016). Due to reduced exposure at the Landfill when sampling was conducted, the part of the sequence sampled for this study is

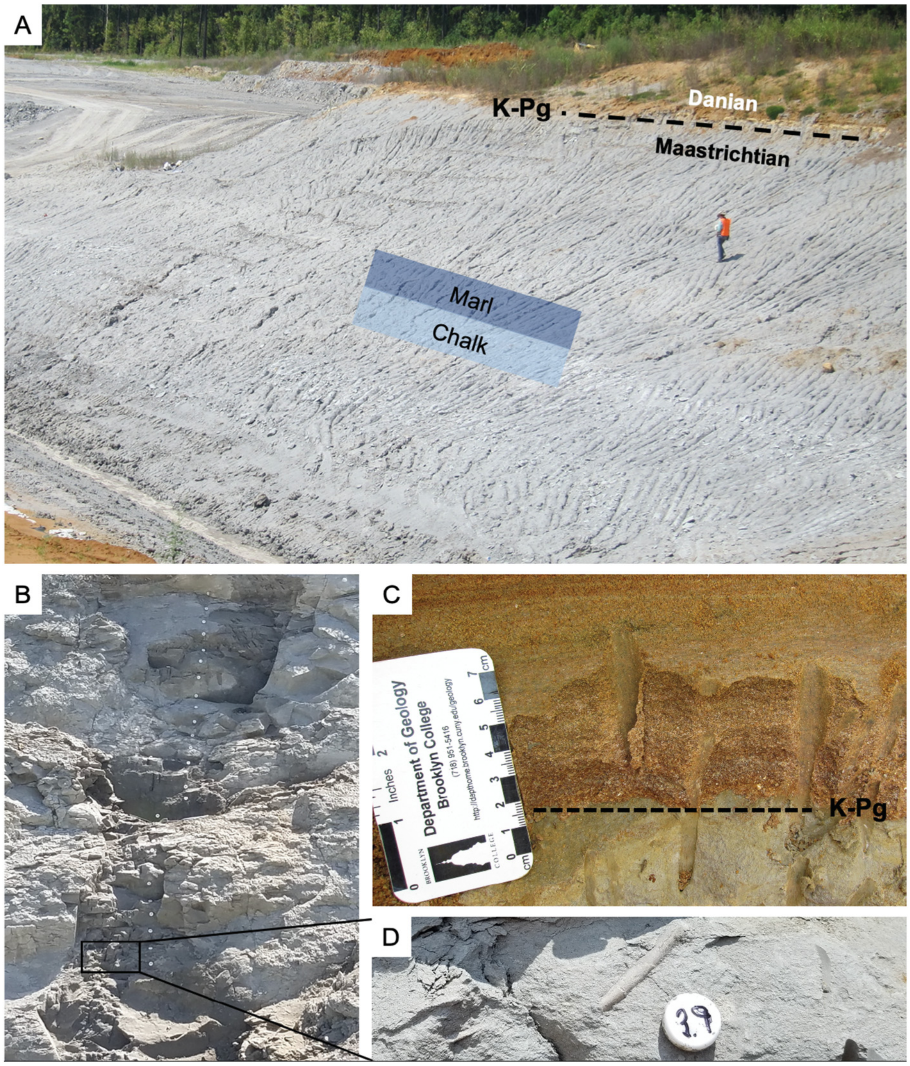

Fig. 4. The Prairie Bluff (PB) Landfill locality A: The section at the PB Landfill. The K–Pg boundary is outlined in dashed black line. Chalk and marl alteration in outcrop is indicated by light (chalk) and dark (marl) blue. B: Part of the sampled section with white pins marking 10 cm intervals. C: Close-up of the K–Pg boundary marked in dashed black line. D: *Eubaculites carinatus* in situ 3.9 m below the K–Pg boundary toward the base of the section shown in B. (For interpretation of the references to color in this figure legend, the reader is referred to the web version of this article.)

restricted to the top 6.5 m of the upper Maastrichtian (Fig. 6). Calcareous nannofossil *Lithraphidites quadratus* and dinoflagellate *P. grallator* occur throughout the section (Larina et al., 2016). Based on the occurrence of *L. quadratus* at the base of the section, the PB Landfill is assigned to the UC20a^{TP} subzone. However, other biostratigraphic markers such as *P. grallator* and *D. iris* suggest a latest Maastrichtian age. No new analyses for calcareous nannofossils were conducted for the PB Landfill; we refer to the results of Larina et al. (2016) for this section.

4. Methodology

4.1. Field and laboratory methods

The Starkville and PB Landfill sections span 8.2 m and 6.5 m, respectively. Bulk sediment samples were collected in 0.1 m increments. A total of 149 samples were analyzed at the UC Santa Cruz Stable Isotope Facility to obtain $\delta^{13}C_{carb}$ and $\delta^{18}O_{carb}$ values of bulk sediments. Samples were analyzed with a Fisons Prism III dual-inlet isotope ratio mass spectrometer (IRMS). Prior to IRMS analysis, bulk sediment samples were digested using an acid bath. Carbon dioxide gas and water were produced by reacting samples in orthophosphoric acid at 90 °C. Water and non-condensable gases were removed to isolate the CO_2 gas prior to analysis. The CO_2 gas was then analyzed with the IRMS. An autocarbonate device pressure transducer has been calibrated to carbonate mass, thus providing wt%$CaCO_3$ data simultaneously with stable isotope values of bulk sediments. The calibrated Carrera Marble standard was used to correct $\delta^{13}C_{carb}$ and $\delta^{18}O_{carb}$ values. We report stable isotope data with respect to the Vienna Pee Dee Belemnite (V-PDB) standard.

Prior to pXRF analysis, approximately 100 g of each sample was homogenized into a fine powder by grinding with a porcelain mortar and pestle. Cross sample contamination was avoided by washing the mortar and pestle with deionized water and acetone prior to each grinding. The powdered samples were transferred into plastic bags and pressed into ~4×5 cm pods. Elemental concentrations of Fe, Ti, K, Sr and Ca were obtained from all samples using an Olympus Innov-X X-ray fluorescence (pXRF) portable hand apparatus. For each sample, elemental data were collected for a total of 90 s set to 30 kV and 50 kV beams. The certified NIST 2710 standard was scanned every 20 runs. The analysis was conducted in the Environmental Science Analytical Center (ESAC) at CUNY Brooklyn College. A single non-carbonate standard was available for these analyses, therefore, absolute values of elemental concentrations may not be reliable. However, relative changes in elemental concentrations show shifts that match lithological changes well in both locations, and thus were used for correlation and cyclostratigraphic analysis.

Seven samples from the PBC and one from the Clayton Fm of the Starkville section were analyzed for calcareous nannofossils. Standard smear-slides were prepared. Ten to twenty fields were examined in order to count the total number of specimens per field of view as well as relative abundances of taxa; relative abundances were calculated across a range of total specimens per sample from a minimum of 244 up to 474 total specimens for Maastrichtian samples while only 149 specimens were counted in the Danian sample. No evaluation of species richness was performed. Taxa were grouped by genera, except for *Prediscosphaera stoveri* which was counted separately from other *Prediscosphaera*. Fig. 11 reports sampling intervals and the occurrence of relevant biostratigraphic markers (e.g. *Micula prinsii*). No new analysis for calcareous nannofossils was conducted on PB Landfill sediments; we refer to the results of Larina et al. (2016) for this section.

4.2. Analytical methods (time-series analysis)

To test for the presence of orbital cycles in the PBC, a time-series analysis was conducted on $\delta^{13}C_{carb}$ and $\delta^{18}O_{carb}$ values, wt%$CaCO_3$, and elemental concentrations (Ca, Sr, K, Ti, Fe). Data preparation and spectral analyses were conducted using the stand-alone software *Acycle* (Li et al., 2019). Prior to spectral analyses, each dataset was interpolated using a sampling rate of 5 cm. To eliminate long-term trends, all datasets were detrended using robust locally weighted regression smoothing (rLOESS) with a window length of 35%. Spectral analysis was conducted on all datasets using the Multi-Taper Method (MTM; Thomson, 1982). Two tapers were selected for this study. Robust red noise estimation (Mann and Lees, 1996) provided confidence levels of 99.9%, 99%, 95% and 90%. Frequency changes throughout each dataset were detected using evolutionary power spectra (Kodama and Hinnov, 2015) with a sliding window length of 2.3 m and a step of 0.1 m. Cycles were extracted using the Gaussian band-pass filter technique (Kodama and Hinnov, 2015), based on significant frequencies (>95% confidence level) provided by the MTM analysis.

5. Results

5.1. Chemostratigraphy

5.1.1. Starkville section (AMNH loc. 3525)

All proxies exhibit large-scale trends (described below) overprinted by smaller fluctuations that reflect cyclical changes in lithology. $\delta^{13}C_{carb}$ values range from 0.37‰ to 1.33‰ (mean 0.8‰). The basal 4 m of the section exhibits a steady increase from a minimum value 0.4‰ to 1.2‰. This is followed by a decrease and a subsequent increase to a maximum value of 1.33‰ between 4 m and 6 m. Values decrease to 0.57‰ at the K–Pg boundary (Fig. 5A). $\delta^{18}O_{carb}$ records from Starkville exhibit several large-scale shifts (Fig. 5A). Values range from −2.8‰ to −1.7‰ (mean −2.3‰). A general decrease occurs between 0 and 4 m. The interval between 4 and 6 m exhibits an increase to a maximum value of −1.7‰, followed by a decrease to −2.2‰ throughout the rest of the section. In general, a high correlation between $\delta^{13}C_{carb}$ and $\delta^{18}O_{carb}$ implies some degree of diagenetic alteration. At Starkville, low covariance between $\delta^{13}C_{carb}$ and $\delta^{18}O_{carb}$ ($R^2 = 0.051$), in conjunction with good calcareous nannofossil preservation, suggests that sediments have not undergone significant diagenetic alteration (Fig. 5B; Mitchell et al., 1997; Thibault et al., 2016a; Huck et al., 2017).

Weight %$CaCO_3$ from the Starkville locality ranges from 44 to 93% with a mean of 68%. An increase from ~60 to 90% occurs in the basal ~3 m, followed by a gradual decrease to a ~50% at 6 m and a subsequent increase to ~60% up to the K–Pg boundary. Generally, carbonate phase elements (Ca, Sr) are inversely correlated with Fe, Ti and K, representing the siliciclastic fraction (Fig. S1). In agreement with other proxies, element

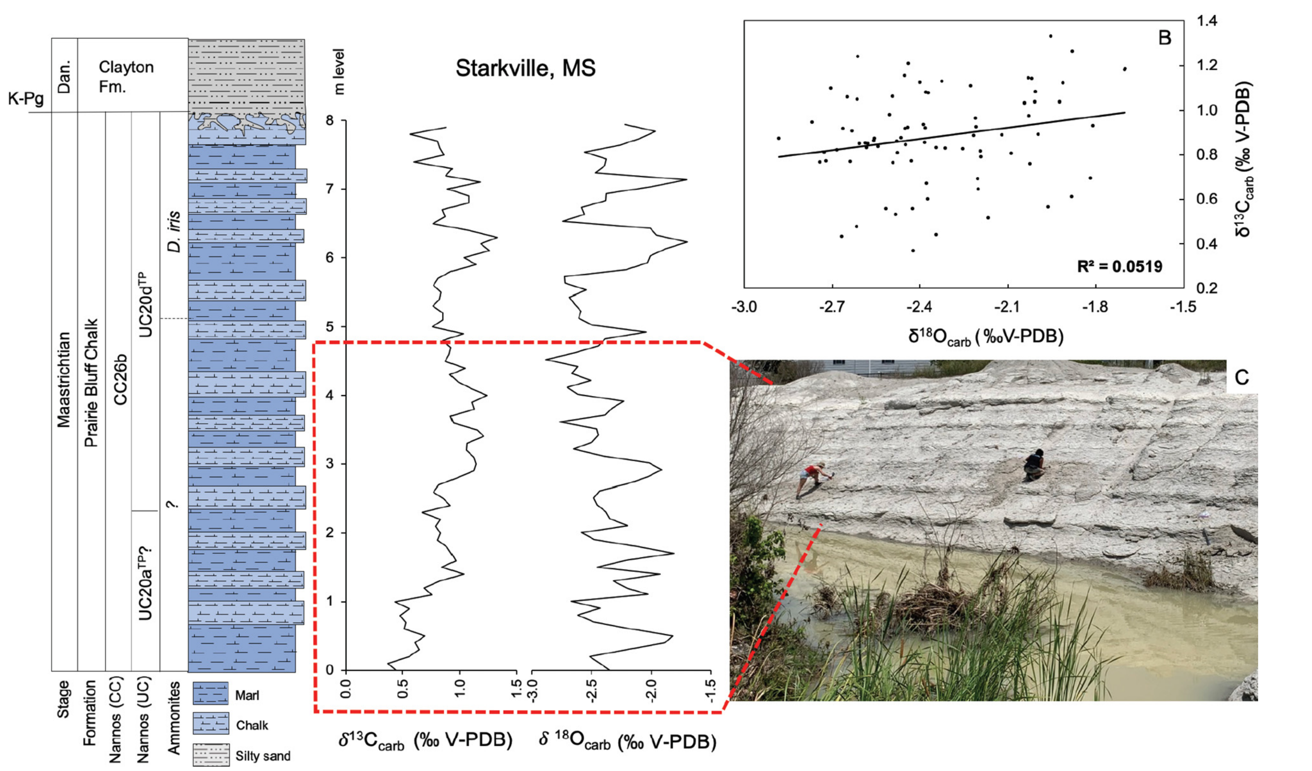

Fig. 5. A: Biostratigraphy, lithostratigraphy and stable isotope data from Starkville, Mississippi. B: Cross-plot of $\delta^{18}O_{carb}$ vs. $\delta^{13}C_{carb}$ ($R^2 = 0.05$). C: Basal ~5 m of the section corresponding to the part of the record outlined in dashed red. (For interpretation of the references to color in this figure legend, the reader is referred to the web version of this article.)

records show several large-scale trends in addition to small scale shifts that represent chalk–marl alterations. Fe (%), Ti (ppm) and K (%) exhibit similar trends throughout the section with a gradual, decreasing trend between 0 and 4 m. This is followed by a rapid increase between 4 and 6 m and a slight decrease in values up to the K–Pg boundary (Fig. S2). Carbonate-phase elements (Sr, Ca) show somewhat similar trends to wt%$CaCO_3$, however, large scale trends in the upper half of the section are not as apparent. Sr and Ca exhibit a general increasing trend from 0 to 4 m followed by a decreasing trend up to the boundary (Fig. S2).

5.1.2. Prairie Bluff Landfill (AMNH loc. #3483)

$\delta^{13}C_{carb}$ records from the PB Landfill exhibit high-amplitude variations between chalk and marl beds (~1‰) compared to Starkville. $\delta^{13}C_{carb}$ values range from −0.05 to 1.45‰ with a mean of 0.75‰. Like the Starkville section, chalks exhibit more depleted $\delta^{13}C_{carb}$ values compared to the marls (Fig. 6A). In accordance with $\delta^{13}C_{carb}$, $\delta^{18}O_{carb}$ values are characterized by large changes between chalk and marl beds (typically >1‰), which may suggest diagenesis due to interaction with meteoric water. $\delta^{18}O_{carb}$ range from −3.2‰ to −1.3‰ with a mean of −2.1‰. Generally, chalks show more depleted values compared to marls (Fig. 6A). A high covariance ($R^2 = 0.70$) between $\delta^{13}C_{carb}$ and $\delta^{18}O_{carb}$ in addition to unrealistic $\delta^{18}O_{carb}$ fluctuations suggests that PB Landfill sediments have undergone some degree of diagenetic alteration (Fig. 6B; Mitchell et al., 1997; Jarvis et al., 2015). Consequently, $\delta^{13}C_{carb}$ and $\delta^{18}O_{carb}$ data from the PB Landfill were not used for correlation purposes or environmental reconstruction. Instead, wt%$CaCO_3$ and XRF records of Ti and K were used to correlate the PB Landfill section with Starkville.

At the PB Landfill, wt%$CaCO_3$ values range from 22 to 79% with a mean of 43%. Wt%$CaCO_3$ is characterized by several large-scale shifts superimposed by cyclical variations. The basal 1.5 m decreases in wt%$CaCO_3$ from ~60% to a minimum of 22%. This is followed by a gradual increase toward the K–Pg boundary. Generally, Ti, Fe and K exhibit an increasing trend from 0 to 2 m. This is followed by a decrease in values up to the K–Pg boundary (Fig. S3). As supported by similar trends observed in the wt%$CaCO_3$, Ti and K as described further below, we find that the basal approximately 4.7 m of the PB Landfill is correlative to the topmost ~3.3 m of Starkville (Fig. 7).

5.2. Cyclostratigraphy

5.2.1. Cyclostratigraphy in the Starkville section

Spectral estimation reveals several prominent frequency peaks observed in power spectra obtained from geochemical data. Multi-Taper-Method (MTM) results indicate spectral peaks within two distinct frequency bands above the 99.9% confidence interval (CI; Fig. 8). $\delta^{13}C_{carb}$, $\delta^{18}O_{carb}$, wt%$CaCO_3$ and detrital elements (Ti, K) show distinct peaks within a low frequency band centered around 0.90 cycles/m, indicating a periodicity of 1.1 m (cycles). Several proxies (wt%$CaCO_3$, Ti, K) show significant (>99% CI) peaks within a high frequency band centered at 1.80 cycles/m, representing a periodicity of 0.55 m; this is also the approximate thickness of couplets at this locality. Fe also shows peaks within this frequency band (>99% CI); however, Fe is characterized by a wide range of frequencies in the high frequency portion of the spectrum, and is thus difficult to interpret (Fig. S4). Carbonate phase elements (Ca, Sr) reveal somewhat similar results, but spectral peaks are not as prominent (<95% CI) and are spread out over a wider range of frequencies compared to Ti, K and stable isotopes. Power spectra for Ti, wt%$CaCO_3$ and stable isotopes are shown in Fig. 8 (see Fig. S4 for power spectra of all other proxies).

Changes in frequency patterns throughout the section were determined using evolutionary power spectral analysis (Fig. 8). The lower frequency band is most pronounced in the basal ~4 m of the section. Above this meter level, wt%$CaCO_3$ power spectra indicate a distinct shift from solely low frequency signals between 0 and 4 m to a higher frequency band centered around 1.80 cycles/m. The 1.1 m periodicity

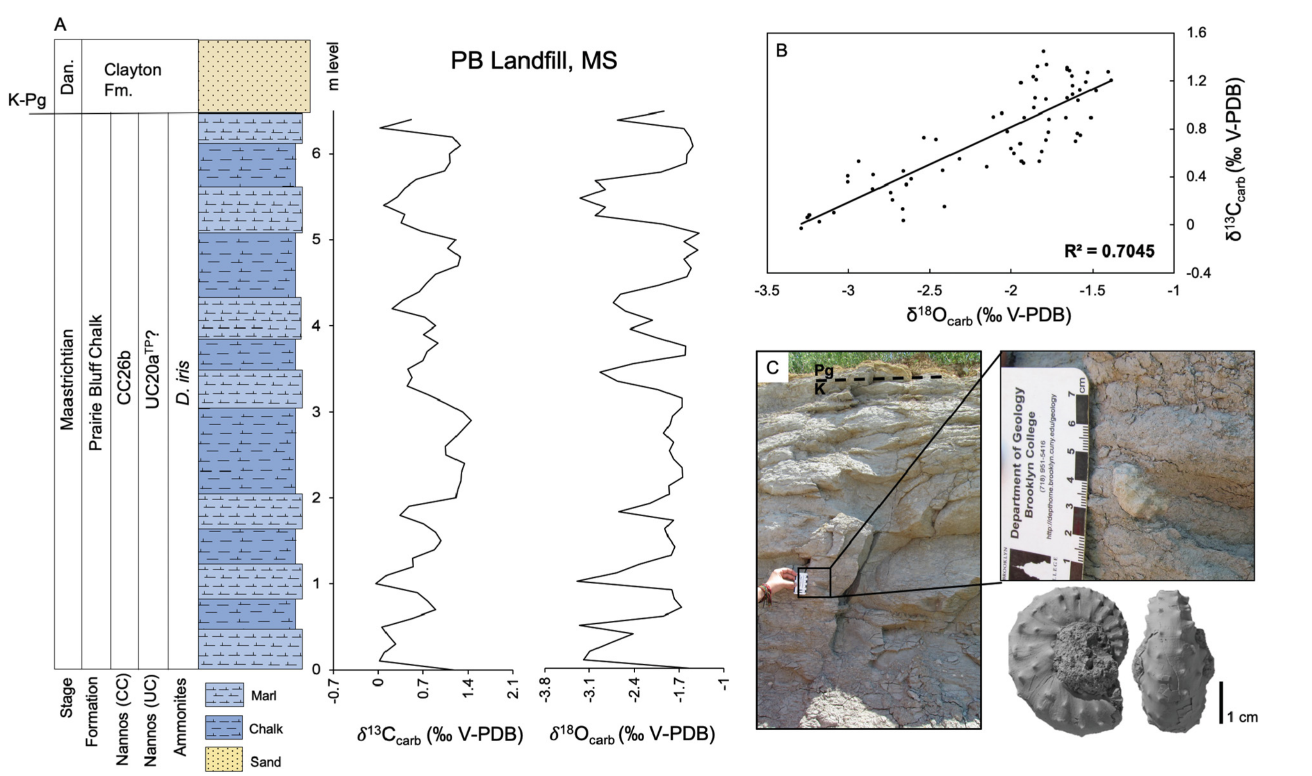

Fig. 6. A: Biostratigraphy, lithostratigraphy and stable isotope profiles from the PB Landfill. B: Cross–plot of $\delta^{13}C_{carb}$ and $\delta^{18}O_{carb}$ ($R^2 = 0.7$). C: *Discoscaphites iris* in situ ~1 m below the K–Pg boundary. Bottom right image: *D. iris* modified from Larina et al. (2016).

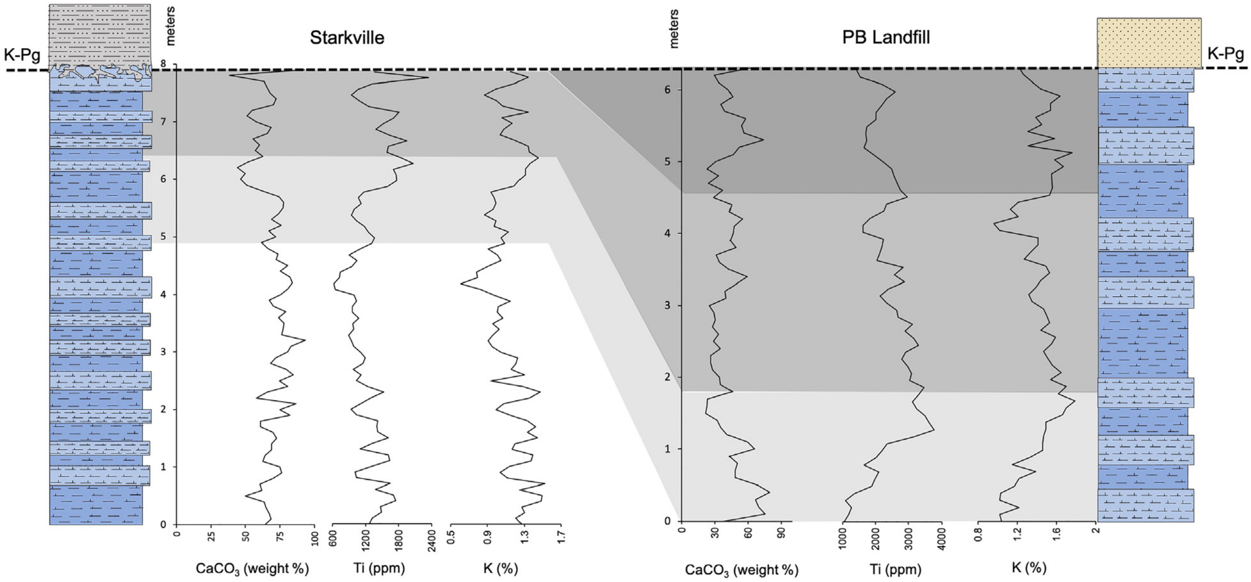

Fig. 7. Correlation of the Starkville section with the PB Landfill based on wt% $CaCO_3$, Ti and K concentrations. Correlative records are highlighted in light gray. The area highlighted in dark gray at the top of the PB Landfill is not preserved at Starkville and most likely represents ~2 precession cycles. Error margins for elemental proxies (1 sigma error) are reported in Supplementary data.

returns to a higher power toward the top of the section ~1.5 m below the K–Pg boundary, where both frequencies occur at high powers (Fig. 8). Ti and K records exhibit high power in both frequency bands in the basal ~1.5 m of the section (Fig. 8; Fig. S4). In accordance with wt%$CaCO_3$, the 0.90 cycles/m frequency band dominates the middle–upper (~1.5–4.5 m) part of the section, above which 1.80 cycles/m frequency band returns to high powers. The Gaussian bandpass filter technique was used to extract cycles from the time-series with peaks >99% CI (Fig. 9). Wt%$CaCO_3$, Ti, and K filter outputs show distinct amplitude modulation of the high-frequency band which is commonly attributed to the effects of eccentricity on precession (Huybers and Aharonson, 2010; Westphal et al., 2010; Meyers, 2015). We observe ~5 cycles within each amplitude envelope, consistent with the short eccentricity–precession ratio of 1:5. Gaussian filter outputs for Ti and wt% $CaCO_3$ are shown in Fig. 9. Filter outputs for the remaining proxies are provided in Fig. S5.

5.2.2. Cyclostratigraphy in the Prairie Bluff Landfill section

Time-series analysis of detrended proxy data from the PB Landfill indicates significant spectral peaks within a single frequency band centered around 1.31 cycles/m in $\delta^{13}C_{carb}$, $\delta^{18}O_{carb}$, wt%$CaCO_3$, Ti, K and Fe records (>99.9% CI; Fig. 10). This frequency band corresponds to a periodicity of 0.76 m, which generally matches the approximate thickness of couplets observed in outcrop (Fig. S7). As observed in the Starkville locality, spectral estimation of carbonate phase elements (Sr, Ca) shows a spread over a wide frequency range, resulting in broad spectral peaks that do not stand out like those obtained from other proxies (Fig. S6) Overall, proxy records from the PB Landfill reveal significant, distinct periodicities within a single frequency band centered around 1.31 cycles/m.

Evolutionary power spectra of stable isotopes and wt%$CaCO_3$ reveal a single, dominant frequency band centered around ~1.31 cycles/m (Fig. 10). This band shifts from lower frequencies in the basal part of the sequence (0.9 cycles/m), to higher frequencies (1.6 cycles/m cycles/m) up section (Fig. S6). Fe and Ti show the opposite, with a dominant and consistent frequency band centered at ~1.31 cycles/m with shifts from higher to lower frequencies up section. Evolutionary power spectra of Ti reveal a concentration of power within the same frequency band as $\delta^{13}C_{carb}$, $\delta^{18}O_{carb}$, wt%$CaCO_3$, and Fe (1.31 cycles/m). Sr and Ca also show a concentration of power within the dominant frequency band; however, the wide range of frequencies across these spectra make it difficult to interpret (Fig. S6).

5.3. Calcareous nannofossils

The preservation of the calcareous nannofossil assemblage is moderate to good in all samples of the section, and very well preserved at the 5.7 m level. The total nannofossil abundance remains high and fairly stable throughout the Maastrichtian part of the section, regardless of the lithology (i.e., marls versus limestones), and fluctuating around 25 specimens per field of view (N/FOV). A large drop in abundance is recorded in the Danian sample reaching down to 7.5 N/FOV (Fig. 11).

The Maastrichtian assemblage is dominated by *Prediscosphaera* spp., *Micula* spp., *C. ehrenbergii*, *Watznaueria* spp., *P. stoveri* and *Arkhangelskiella* spp. (Fig. 11). There is no clear correlation between the relative abundance of the most resistant species in the assemblage, *Micula* spp., and the total abundance. The percentage of this species generally remains below 30%, except for one sample. Therefore, we consider that the composition of the assemblage has not been significantly altered by diagenesis (Thibault and Gardin, 2006). The most significant change observed in the assemblage across the Maastrichtian is expressed by a rapid increase in the relative abundance of *C. ehrenbergii*. This taxon is a minor component of the assemblage below 4 m but becomes one of the dominant taxa (>10%) from 5 m to the top of the section. This change is also paralleled by a relatively lower abundance of *Micula* spp., *Watznaueria* spp. and *Arkhangelskiella* spp. up section while minor components of the assemblage such as zeugrhabdotids (*Placozygus* and *Zeugrhabdotus* spp.), *Chiastozygus* spp. and *Microrhabdulus* spp. increase (Fig. 11). The Danian sample is characterized by a marked increase in the relative abundance of *Cervisiella operculata* fragments, which is a typical feature of early Danian sediments (Gardin, 2002).

This additional sampling has yielded significant new biostratigraphic information that better constrains the age of the Starkville section (Fig. 11). *Micula prinsii*, the global index species for the uppermost Maastrichtian, was recovered from 5.7 m and 3 m levels below the K–Pg boundary. Based on these occurrences, the

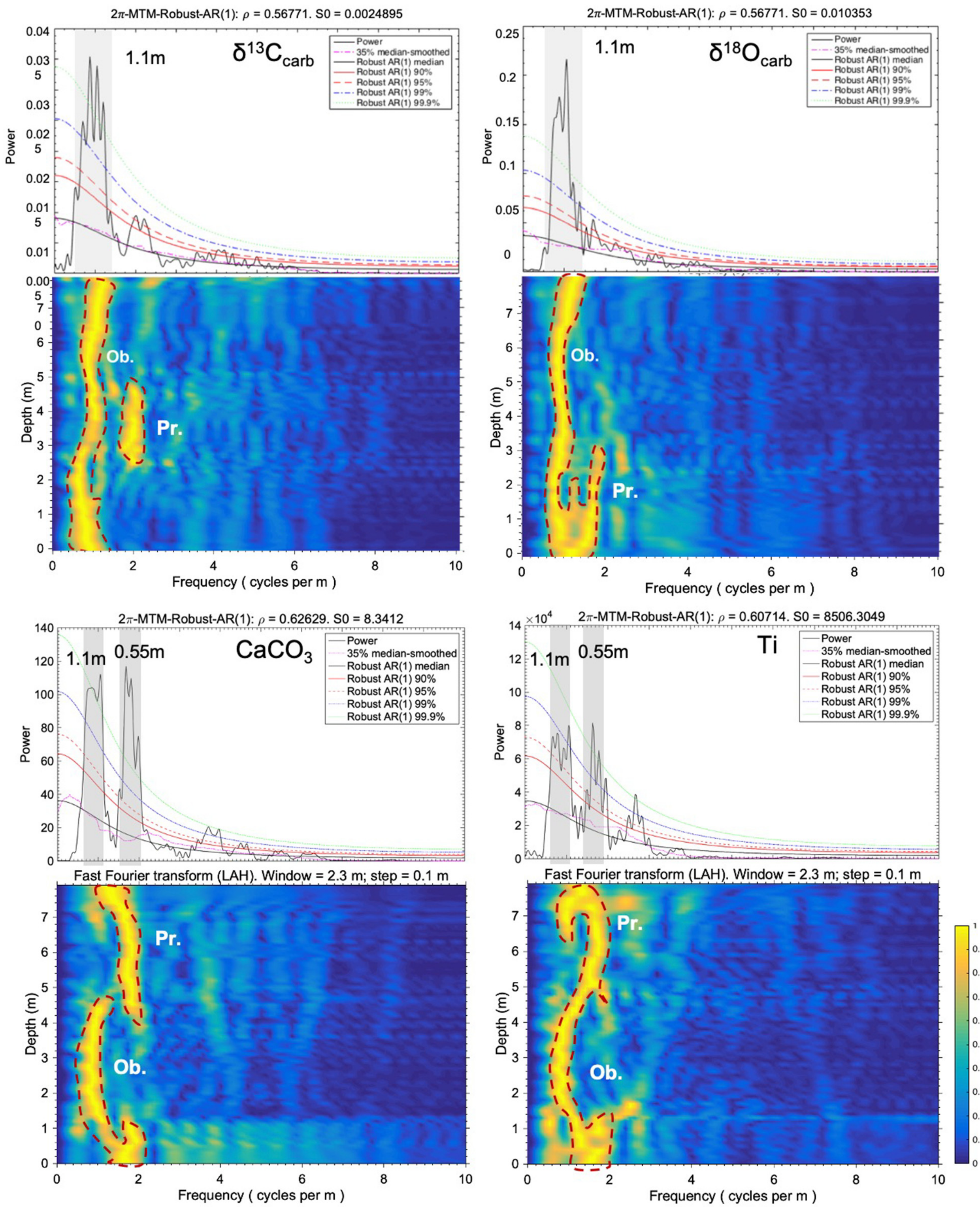

Fig. 8. Spectral analysis results from Starkville. MTM power spectra and evolutionary power spectra for $\delta^{13}C_{carb}$, $\delta^{18}O_{carb}$, %$CaCO_3$ (wt%) and Ti. K, Fe, Sr and Ca spectrograms are included in Supplementary material. K, Fe, Sr and Ca do not exhibit peaks above the 99.9% confidence interval with the exception of K (0.55 m peak exceeded 99.9%) and generally show large spread in spectra with less definitive peaks. Significant spectral peaks and corresponding cycles of the proxies shown here are highlighted in light gray. These peaks represent periodicities of 1.1 m (frequency 0.90 cycles/m) and 0.55 m (1.80 cycles/m). Biostratigraphic constraints and a frequency ratio of 2:1 suggest obliquity and precession cycles, respectively. Rho (ρ) is the lag − 1 autocorrelation coefficient and S_0 represents the average power.

top ~5.7 m of the Starkville section is assigned to the UC20d^{TP} subzone (Fig. 5A). The lower part of the section is more difficult to constrain. Based on the absence of *Micula murus* and *Ceratolithoides kamptneri*, markers for the UC20b^{TP} and UC20c^{TP} subzones, and the presence of *L. quadratus*, this interval is assigned to the UC20a^{TP} subzone. However, as noted above, the absence of marker taxa for zones UC20b^{TP} and UC20c^{TP} is most likely a result of environmental factors rather than erosion and/or non-deposition.

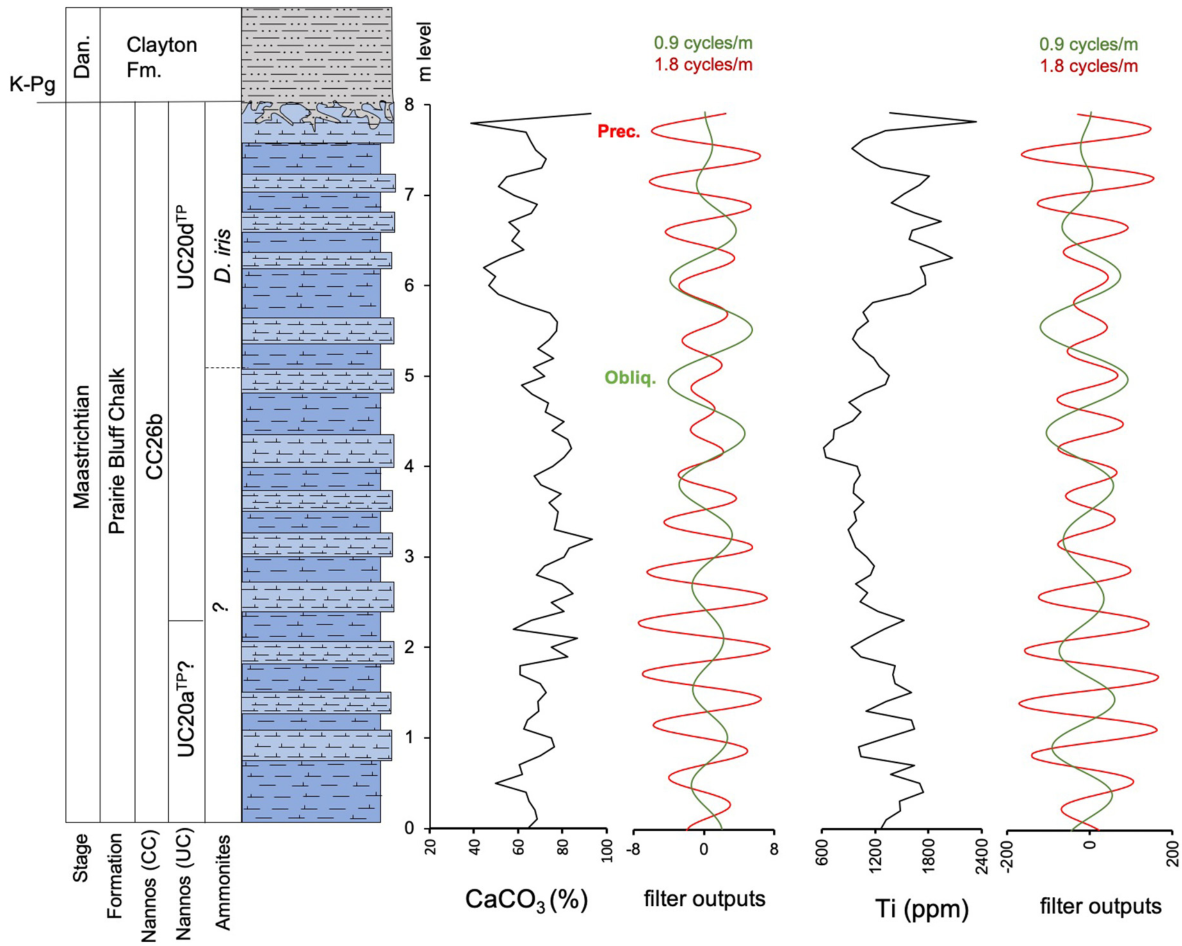

Fig. 9. Integrated biostratigraphy, lithostratigraphy, chemostratigraphy and cyclostratigraphy from Starkville. Carbonate content (wt%$CaCO_3$), Ti, and K concentration profiles correspond to precession filter outputs outlined in red (0.55 m cycles), and obliquity filters outlined in green (1.1 m cycles). These correspond to significant frequency bands centered around 1.8 ± 0.3 cycles/m and 0.9 ± 0.2 cycles/m, respectively. (For interpretation of the references to color in this figure legend, the reader is referred to the web version of this article.)

6. Discussion

6.1. Astronomical forcing and sedimentary cyclicity in the Prairie Bluff Chalk

Ammonite and microfossil biostratigraphy constrains the likely duration of both sections to ~200–400 kyr, limiting primary cycle possibilities to obliquity and precession, which typically have a ratio of 2:1 (Laskar et al., 2004). To determine which cycles dominate deposition in the Maastrichtian GCP, we obtained frequency ratios based on significant spectral peaks (Weedon, 2003; Strasser and Heckel, 2007; Thibault et al., 2016a). Distinct peaks in power spectra show a 2:1 ratio of dominant frequencies in wt%$CaCO_3$, Ti, and K data from Starkville (Fig. 8). The high frequency band centered around 1.80 cycles/m (0.55 m cycles), most likely corresponding to precession cycles, represents the rhythmites in outcrop (Figs. 1A, 12). We interpret the lower frequency band (0.90 cycles/m), which represents a 1.1 m periodicity, to be obliquity cycles. Due to the short length of the sampled record and a single significant frequency band, frequency ratios cannot be applied to the PB Landfill section. Consequently, we identified Milankovitch cycles at the Landfill using correlation with Starkville. Based on biostratigraphic constraints, spectral estimation and correlation, rhythmic sedimentation at the PB Landfill was also likely controlled by precession cycles. This is consistent with the precession component being dominant at subtropical locations (Bosmans et al., 2015; Figs. 1A, 12). However, the likelihood of obtaining a Milankovitch-scale ratio in sedimentary data is high, thus a record long enough to express multiple frequency ratios is necessary to be sure (Waltham, 2015). To improve this cyclostratigraphic interpretation, both GCP sections should be sampled further down to obtain a longer record. Unfortunately, exposure is limited below our lowest data points at both sections, constraining the extent to which these data could be expanded temporally.

Despite this, our cyclostratigraphic correlation and biostratigraphic constraints allow for preliminary astronomical cycle identification in the Prairie Bluff Chalk. Cycle counting based on filter outputs suggests 14 and 8 precession cycles at Starkville and the PB Landfill, respectively. These correspond well with the number of rhythmites observed in outcrop at both localities. Based on the average estimate for the length of climatic precession during the Late Cretaceous (66 Ma; ~20.6 kyr; Waltham, 2015; Berger et al., 1992), the estimated duration of the section sampled at Starkville (8 m thick) is ~300 kyr. The duration of the measured sections at the PB Landfill (6.5 m thick) is estimated to be ~165 kyr. These estimates provide average sedimentation rates of ~2.8 cm/kyr and 3.9 cm/kyr for Starkville and the PB Landfill, respectively. The PB Landfill section was probably deposited under higher sedimentation rates than Starkville as suggested by thicker couplets and generally higher concentrations of terrigenous elements such as Ti. This is probably due to its closer proximity to a siliciclastic sediment source.

Bandpass filters for wt%$CaCO_3$, Ti, and K reveal typical amplitude modulation of the high frequency band (1.80 cycles/m; Fig. 9). This pattern is commonly attributed to the effects of short eccentricity on axial

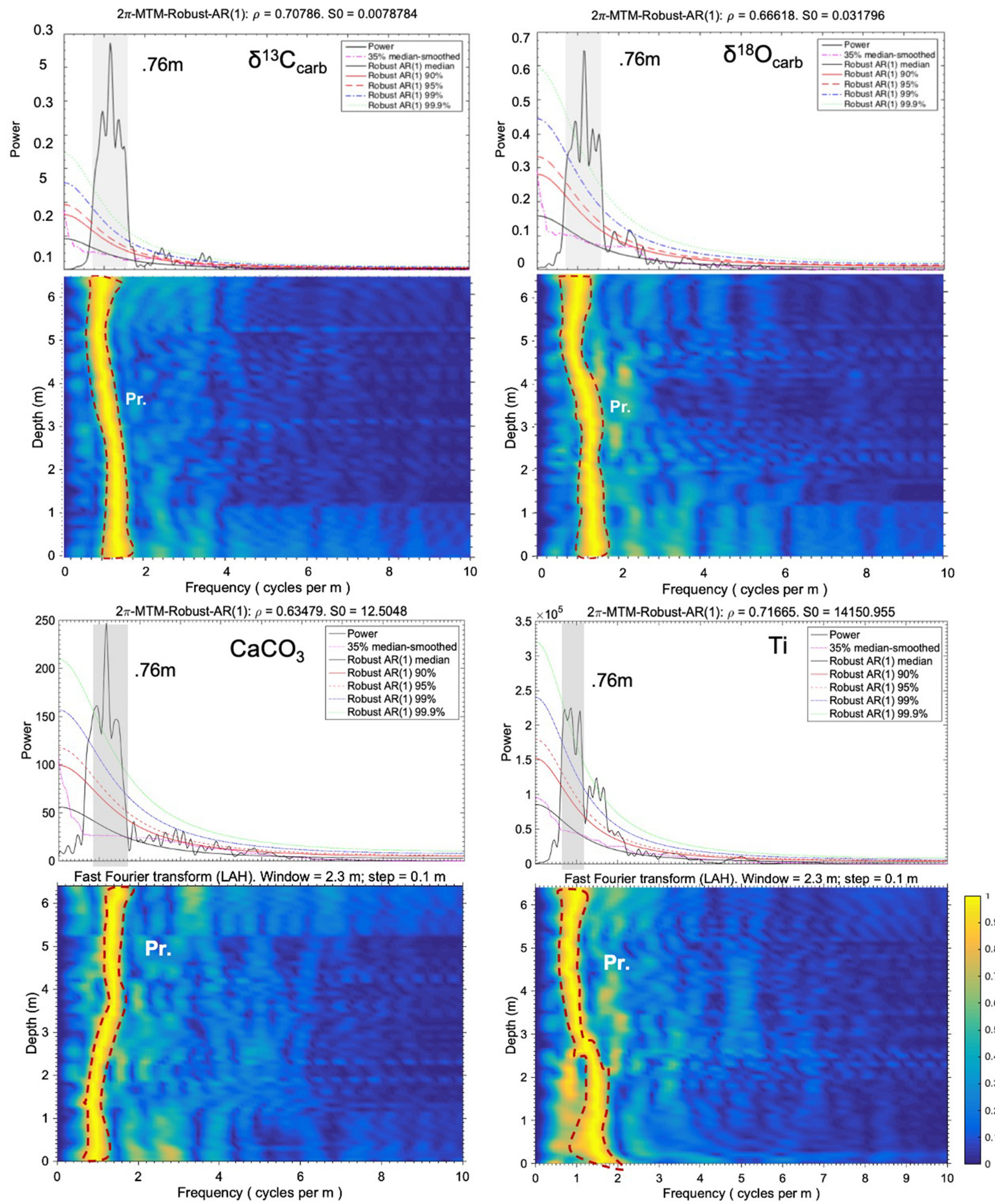

Fig. 10. Spectral analysis results from the Prairie Bluff Landfill. MTM power spectra (top) and evolutionary power spectra for $\delta^{13}C_{carb}$, $\delta^{18}O_{carb}$, $\%CaCO_3$, Fe, and Ti, respectively. Significant spectral peaks and corresponding cycles are highlighted in light gray. Evolutionary power spectra show power with respect to stratigraphy (depth). The frequency band centered around 1.31 cycles/m corresponds to a periodicity of 0.76 m and most likely represents precession cycles.

precession (Huybers and Aharonson, 2010; Meyers, 2015). Although this pattern is a good indicator of short eccentricity cycles, the record is too short to express eccentricity scale frequencies in power spectra. However, cycle counting based on Ti and K filter outputs shows approximately five cycles within one amplitude envelope, which is the typical number of precession cycles within one short eccentricity cycle (~100 kyr). Amplitude modulation in $wt\%CaCO_3$ filters occurs in the basal and upper parts of the section. The weak eccentricity signal in the middle part of the section seems not preserved, thus, overall amplitude modulation of the $wt\%CaCO_3$ filter output does not reveal any conclusive patterns (Fig. 12). If amplitude modulation in Ti and K records was in fact driven by eccentricity, ~3 short eccentricity cycles are preserved within the Starkville section (Fig. 12). This interpretation is in line with the estimated duration calculated from the inferred precession

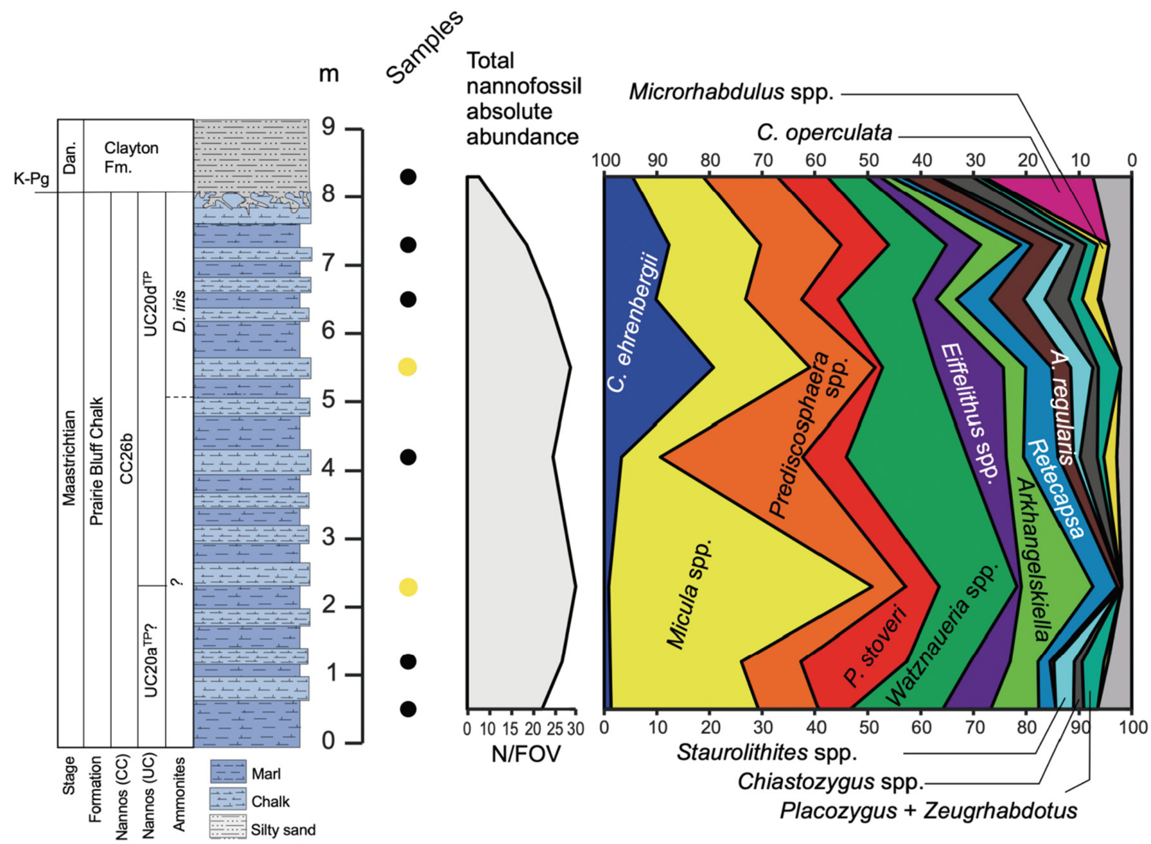

Fig. 11. Composition of the nannofossil assemblage from Starkville depicted by cumulative 922 relative abundance (%). Samples analyzed for nannofossils are marked by circles next to 923 corresponding meter levels. *Micula prinsii* occurrences are marked by yellow circles. (For interpretation of the references to color in this figure legend, the reader is referred to the web version of this article.)

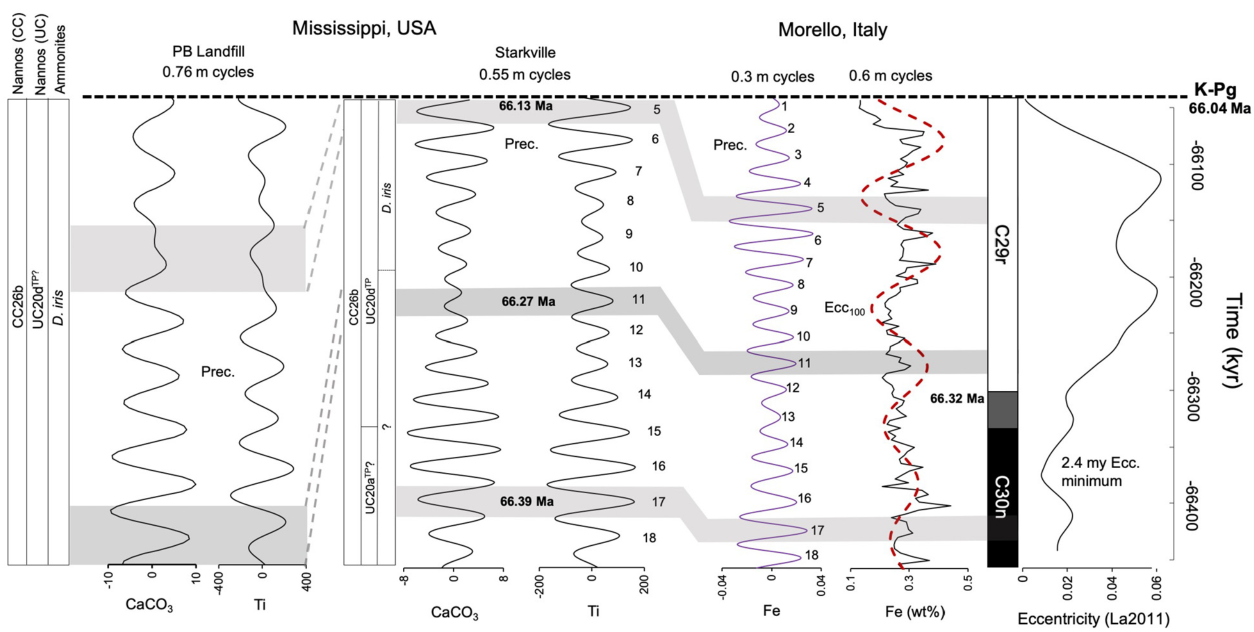

Fig. 12. Approximate age estimates and cyclostratigraphic correlation of the Starkville and PB Landfill sites with the Morello section. Filter outputs represent frequency bands centered around 1.31 ± 0.3 cycles/m ($CaCO_3$ and Ti from the PB Landfill), and 1.80 ± 0.3 cycles/m ($CaCO_3$, K and Ti from Starkville); both are interpreted to represent precession cycles. Precession filter output for Fe (wt%) data in purple (cycles are numbered). Raw Fe (wt%) data (from Sinnesael et al., 2019) and the short eccentricity output (dashed red). Frequency bands from Morello that are centered around 3.0 ± 0.5 cycles/m and 0.7 ± 0.3 cycles/m represent precession and short eccentricity cycles, respectively. ~66.32 Ma represents an age estimate for the C29r/C30 reversal by Sinnesael et al. (2019). Laskar et al. (2011) eccentricity solution (far right) indicating a 2.4 myr eccentricity minimum (modified from Sinnesael et al., 2019). (For interpretation of the references to color in this figure legend, the reader is referred to the web version of this article.)

cycles. Moreover, our correlation to the Morello section (see below) supports similar amplitude modulations of the filter outputs we constructed using Fe (wt%) data from Sinnesael et al. (2019) (Fig. 12). These suggested eccentricity minima also coincide with large scale shifts in wt%$CaCO_3$, $\delta^{13}C_{carb}$, detrital element concentrations, and minimum $\delta^{18}O_{carb}$ values. Thus, large-scale trends in geochemical proxies could in part be driven by orbital forcing. Interestingly, the upper interval at the Starkville section also exhibits a distinct change in calcareous nannofossil and macroinvertebrate taxa (discussed below).

6.2. Correlation with other late Maastrichtian records and construction of a floating timescale for the GCP

Sinnesael et al. (2018, 2019) constructed high-resolution XRF and stable isotope records for several complete, deep water (~1000 m paleodepth) K–Pg boundary sites within the Umbria–Marche basin in Italy, specifically the well-studied Bottaccione site and a new site in Morello (Fig. 1). The first high-resolution carbon isotope chemostratigraphy presented here allows for comparison of the GCP sections with the complete sections of the Umbria–Marche basin, which reveals similar patterns in $\delta^{13}C_{carb}$ profiles. Although absolute carbon isotope values differ (as expected for shallow marine vs. deep water carbonates), strong similarities are evident in carbon isotope trends and general patterns (Fig. 13). $\delta^{13}C$ trends observed in this study and both sections in Italy (Sinnesael et al., 2019) are also consistent with upper Maastrichtian carbon isotope records from Elles, Tunisia (Thibault et al., 2016a; Keller et al., 2020) and the latest Maastrichtian of the Newfoundland margin (Batenburg et al., 2017) suggesting our data are consistent with global signals.

Sinnesael et al. (2019) identified precession, obliquity and short eccentricity cycles in Fe (wt%) data from the Morello section. We filtered the Fe (wt%) data based on periodograms provided by Sinnesael et al. (2019) to obtain precession and short eccentricity filter outputs (Fig. 12). We then correlated the Morello section with Starkville at the precession scale by comparison of filter outputs from this study (specifically wt%$CaCO_3$, Ti and K) to that of the filter outputs of Fe (wt%) data from Sinnesael et al. (2019) (Fig. 12). Our filter outputs for wt%$CaCO_3$, Ti and K compare well with Fe (wt%) filter outputs from Morello. Additionally, evolutionary power spectral analysis of proxy data from Starkville reveals similar patterns to Morello and Bottaccione with regard to frequency changes throughout the section. Wt%$CaCO_3$, Ti and K results show a transition from a potential obliquity signal (0.90 cycles/m) in the lower part of the section to a potential precession band (1.8 cycles/m) in the topmost ~4 m of the section. Sinnesael et al. (2018) revealed the same pattern in evolutionary power spectra of pXRF derived Ca, Fe, K data and $CaCO_3$ content in correlative strata from the Bottaccione section in Italy. They found an obliquity-dominated signal in the basal 3 m of the section with a shift to precession and eccentricity dominated spectra in the topmost ~3 m of the Maastrichtian. Although shifts in evolutionary power spectra can occur as a result of changing sedimentation rates, there is no evidence to suggest any change in sedimentation rates at Starkville. However, we do note a transition toward more proximal conditions as indicated by paleontological and geochemical data (see Section 6.3 below).

Our cyclostratigraphic correlation with Morello provides some estimate for the duration of the Maastrichtian portion of the K–Pg unconformity in these GCP successions. Given that the K–Pg boundary section in Morello is considered complete (Sinnesael et al., 2019), our correlation of distinct precession cycles to this section suggests that ca. 4 cycles (~80 kyr) are missing in the upper Maastrichtian at the Starkville locality. Subsequently, chemo- and cyclostratigraphic correlation of the PB Landfill to Starkville sections suggests ~1 cycle (~20 kyr) is missing from the upper Maastrichtian at the PB Landfill (Fig. 12). As noted above, magnetostratigraphic analyses have yet to be conducted on these sections to provide absolute age control. However, based on our correlation with the Morello section and the most recent absolute and estimated ages for the base of magnetochron C29r (between 66.26 and 66.32 Ma; Sprain et al., 2018; Sinnesael et al., 2019; Eddy et al., 2020), we propose that the Starkville section encompasses the C30n/C29r reversal boundary, which should be situated ca. 5 m below

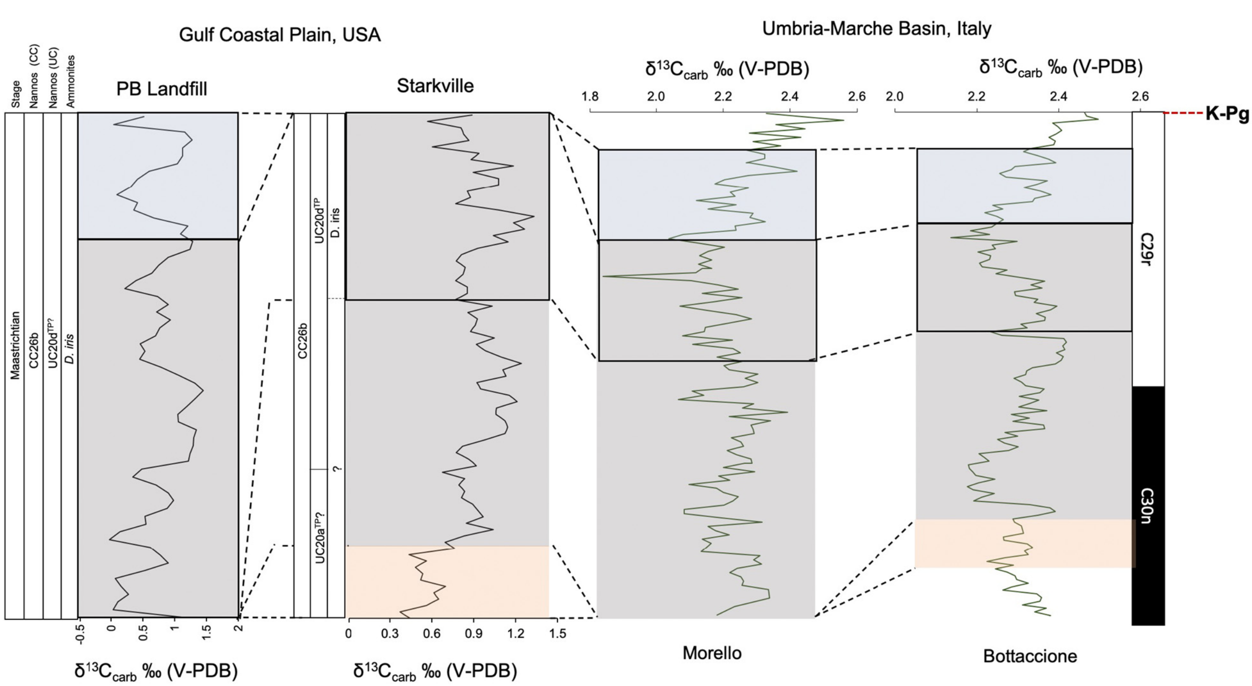

Fig. 13. Biostratigraphy and carbon isotope stratigraphy from the PB Landfill and Starkville correlated with K–Pg sections in Bottaccione and Morello, Umbria–Marche basin, Italy. Carbon isotope data and magnetostratigraphy from Bottaccione and Morello were obtained from Sinnesael et al. (2016, 2019). The y-axis represents depth. These correlations show a more expanded section in the GCP (especially the PB Landfill), compared to Morello and Bottaccione. Correlative isotope shifts are indicated by dashed lines and gray, blue and pink shading. (For interpretation of the references to color in this figure legend, the reader is referred to the web version of this article.)

the K–Pg boundary. The whole sampled PB Landfill section is interpreted to be deposited within chron C29r (Figs. 12, 13).

Although the biostratigraphically important ammonite *Discoscaphites iris* is preserved only in the upper few meters of the Starkville section, it occurs throughout the entire sampled section at the PB Landfill. Thus, based on our cyclostratigraphy, we can also estimate a minimum duration for the *D. iris* biozone to be ~185 kyr (165 kyr + 20 kyr hiatus at the top of the section). These data provide a tentative constraint on the duration of the highest ammonite zone in North America (*D. iris*) and allow for detailed correlation to all sections along the Gulf and Atlantic Coastal Plains where this zone is present.

6.3. Implications for global environmental change in the late Maastrichtian

Astronomically forced, cyclical changes in our proxy records are overprinted by prominent large-scale trends that represent global climate change in the late Maastrichtian. A late Maastrichtian warming event (LMWE) has been well documented and commonly attributed to Deccan Trap degassing (Thibault and Gardin, 2007, 2010; Thibault and Husson, 2016; Batenburg et al., 2017; Barnet et al., 2018; Barnet et al., 2019). The detailed study of Barnet et al. (2019) reported a warming episode based on proxy records from several orbitally tuned, deep-water sites in the Equatorial Pacific and South Atlantic. Their results show a negative shift of ~1‰ in $\delta^{18}O_{benthic}$ records corresponding to an increase of ~2.5–4 °C associated with a phase of Deccan Trap outpouring that started ~66.34 Ma. $\delta^{18}O_{carb}$ data from Starkville show a similar trend with a decrease of ~1‰ throughout the basal 4 m of the section and agree well with other published $\delta^{18}O_{carb}$ records from the same timeframe (Batenburg et al., 2017; Thibault et al., 2016a, 2016b). Unrealistic $\delta^{18}O$ fluctuations among chalk and marl couplets (>1‰) and a high covariance between $\delta^{18}O$ and $\delta^{13}C$ suggest that the PB Landfill records have been altered. Nevertheless, GCP $\delta^{18}O_{carb}$ records such as those from Starkville might represent a global signal of temperature change that further support our stratigraphic correlation based on other proxies. However, further high-resolution $\delta^{18}O$ records from microfossils are still needed from the GCP sections to make valid temperature comparisons. Several studies found a decrease of ~0.5‰ in $\delta^{13}C$ of bulk carbonates and benthic foraminifera during the LMWE (Barnet et al., 2018; Batenburg et al., 2017), suggesting increased atmospheric CO_2 concentrations and some perturbation to the global carbon cycle. If our floating timescale is correct, Starkville data indicate a decreasing trend of ~0.5‰ in $\delta^{13}C_{carb}$ beginning ~300 kyr prior to the K–Pg. Morello and Bottaccione records show similar changes (Fig. 13).

New calcareous nannofossil analysis of the Starkville section provides additional insight into environmental changes during the last ~300 kyr of the Cretaceous in the GCP. An increase in *C. ehrenbergii* relative abundance during the late Campanian of the Zagros basin (Iran) has been recently associated with a significant lowering of sea-level and interpreted as a potential joint response to both a change toward more proximal settings and a decrease in temperature (Razmjooei et al., 2020). In our dataset, patterns of species that show a higher affinity for high latitudes such as *P. stoveri* or *Arkhangelskiella* spp. (Pospichal and Wise, 1990; Lottaroli and Catrullo, 2000; Thibault et al., 2016b) and *Micula* spp., interpreted by some as an ecological generalist with a preference to cool waters (Watkins and Self-Trail, 2005), show an opposition to that of *C. ehrenbergii*, thus ruling out cooling to explain this trend (Fig. 11). However, the rise in *C. ehrenbergii* is associated with a slight increase in *Microrhabdulus* spp., the latter of which may have had an affinity for shelf deposits (Friedrich, 2005). A peak abundance in zeugrhabdotids across the 5–6 m level marks the transition, increasing in concert with the onset of the increase in *C. ehrenbergii*, suggesting a slight rise in water column fertility. *Watznaueria* spp. do not delineate any clear trend through the section, apart from one peak in abundance at 4 m, but this taxon appears to respond significantly to temperature changes only at high latitudes where it is closer to the boundary of its temperature range (Sheldon et al., 2010; Thibault et al., 2016b).

As stated above, high-latitude taxa *P. stoveri* and *Arkhangelskiella* spp. decrease up section in parallel with a slight increase in *A. regularis*, a species that markedly shows higher abundances during warming episodes in the late Campanian–Maastrichtian of the Boreal realm (Thibault et al., 2016b). Therefore, although depicted by small changes in the assemblage compared to the significant change observed with the rise in *C. ehrenbergii*, a slight warming could be suggested by our nannofossil data for the upper part of the section accompanying the trend toward more proximal conditions. Moreover, the increase in abundance of *C. ehrenbergii* at Starkville is accompanied by a change in abundance of macrofossils and shifts in elemental concentrations. Although absolute values obtained from pXRF analysis may not be reliable, relative shifts show a considerable increase in detrital elements such as Ti and to a lesser extent K (Fig. 9). The correlative interval at the PB Landfill shows coincident increases in Ti, K and Fe (Fig. S3), supporting a shift toward more proximal settings. Finally, the upper part of the section at Starkville is rich in macroinvertebrates, including abundant ammonites. In comparison, only a few invertebrates were recovered from the basal ~5 m of the section. This dramatic change in macroinvertebrate occurrence may represent changes in local environmental conditions such as depth and substrate, in parallel with the change in nannofossil assemblages.

7. Conclusions and significance

This study provides the first cyclostratigraphic framework for the Maastrichtian of the GCP based on new geochemical and biostratigraphic analyses of two sections spanning the K–Pg boundary in Mississippi (Starkville and PB Landfill). These data can be used to evaluate latest Cretaceous environmental change in the US Gulf Coastal Plain within a more refined temporal framework. Based on stable isotope ($\delta^{13}C_{carb}$ and $\delta^{18}O_{carb}$), carbonate content (wt% $CaCO_3$), and elemental concentrations (Fe, Ti, K), precession, obliquity and short eccentricity are demonstrated to be well-preserved at the Starkville locality. Due to the shorter record sampled at the PB Landfill, only axial precession could be identified. Combining chemostratigraphic and new biostratigraphic data, the estimated duration of the section below the K–Pg transition at Starkville is ~300 kyr while the section at the PB Landfill likely represents ~165 kyr. Although we have only established a "floating" timescale for the PBC, our data provide constraints on the duration of the uppermost Maastrichtian *Discoscaphites iris* ammonite biozone (≥~185 kyr) and the K–Pg hiatus in this region, estimated to be ~80 kyr at Starkville and ~20 kyr at the PB Landfill.

The high-resolution cyclo- and chemostratigraphy presented here allows correlation of uppermost Maastrichtian strata within the GCP to other sections worldwide. The Starkville $\delta^{13}C_{carb}$ record shows trends and distinctive shifts that are similar to those of the well-studied Morello and Bottaccione sections in Italy and elsewhere, indicating that global scale carbon isotope signals are preserved in the GCP. A high-resolution timescale in addition to a detailed geochemical record of the PBC provides an excellent stratigraphic foundation for future paleoecological and paleoenvironmental studies of the K–Pg transition in the Gulf Coastal Plain.

Supplementary data to this article can be found online at https://doi.org/10.1016/j.sedgeo.2021.105954.

Declaration of competing interest

The authors declare that they have no known competing financial interests or personal relationships that could have appeared to influence the work reported in this paper.

Acknowledgements

This research was funded by: PSC CUNY (award number 61147-00 49), GCAGS (Gulf Coast Association of Geological Societies) and the

N.D. Newell Fund (AMNH). We acknowledge Carlsbergfondet CF16-0457. We are grateful to Stephanie Rodriguez, Kayla Irizarry, Alison Rowe, and Natalie Dastas for assistance in the field, constructive discussions, and editing. Access to the Prairie Bluff Landfill site was provided by Charlie Gardner. Thank you to Colin Carney and Dyke Andreasen (UC Santa Cruz stable isotope laboratory) for conducting the stable isotope analysis. We warmly thank Aura Naujokaitytė, Vilija Naujokaitienė, and Anya Levy for moral support, proofreading assistance, and for assistance with sample preparation in the laboratory.

References

Abramovich, S., Keller, G., Berner, Z., Cymbalista, M., Rak, C., 2011. Maastrichtian Planktic Foraminiferal Biostratigraphy and Paleoenvironment of Brazos River, Falls County, Texas, U.S.A.". The End-Cretaceous Mass Extinction and the Chicxulub Impact in Texas. Society of Sedimentary Geology 123–156.

Alvarez, L.W., Alvarez, W., Asaro, F., Michel, H.V., 1980. Extraterrestrial cause for the Cretaceous–Tertiary extinction. Science 208, 1095–1108.

Alvarez, S.A., Gibbs, S.J., Bown, P.R., Kim, H., Sheward, R.M., Ridgwell, A., 2019. Diversity decoupled from ecosystem function and resilience during mass extinction recovery. Nature 574, 242–245.

Barnet, James S.K., Littler, K., Kroon, D., Leng, M.J., Westerhold, T., Röhl, U., Zachos, J.C., 2018. A new high-resolution chronology for the late Maastrichtian warming event: establishing robust temporal links with the onset of Deccan volcanism. Geology 46, 147–150.

Barnet, J.S.K., Littler, K., Westerhold, T., Kroon, D., Leng, M.J., Bailey, I., Röhl, U., Zachos, J.C., 2019. A high-fidelity benthic stable isotope record of Late Cretaceous–Early Eocene climate change and carbon-cycling. Paleoceanography and Paleoclimatology 34, 672–691.

Barnosky, A.D., Matzke, N., Tomiya, S., Wogan, G.O.U., Swartz, B., Quental, T.B., Marshall, C., McGuire, J.L., Lindsey, E.L., Maguire, K.C., Mersey, B., Ferrer, E.A., 2011. Has the Earth's sixth mass extinction already arrived? Nature 471, 51–57.

Batenburg, S.J., Friedrich, O., Moriya, K., Voigt, S., Cournède, C., Blum, P., Bornemann, A., Fiebig, J., Hasegawa, T., Hull, P.M., Norris, R.D., Röhl, U., Sexton, P.F., Westerhold, T., Wilson, P.A., 2017. Late Maastrichtian carbon isotope stratigraphy and cyclostratigraphy of the Newfoundland Margin (Site U1403, IODP Leg 342). Newsletters on Stratigraphy 51, 245–260.

Berger, A., Loutre, M.F., Laskar, J., 1992. Stability of the astronomical frequencies over the Earth's history for Paleoclimate studies. Science 225, 560–566.

Bond, D.P.G., Wignall, P.B., 2014. Large igneous provinces and mass extinctions: an update. In: Keller, G., Kerr, A.C. (Eds.), Volcanism, Impacts, and Mass Extinctions: Causes and Effects. vol. 505. Geological Society of America, pp. 29–55.

Bosmans, J.H.C., Hilgen, F.J., Tuenter, E., Lourens, L.J., 2015. Obliquity forcing of low-latitude climate. Climate of the Past 11, 1335–1346.

Bralower, T.J., 2002. Evidence of surface water oligotrophy during the Paleocene-Eocene thermal maximum: nannofossil assemblage data from Ocean Drilling Program Site 690, Maud Rise, Weddell Sea. Paleoceanography 17, 1–15.

Chiarenza, A.A., Farnsworth, A., Mannion, P.D., Lunt, D.J., Valdes, P.J., Morgan, J.V., Allison, P.A., 2020. Asteroid impact, not volcanism, caused the end-Cretaceous dinosaur extinction. Proceedings of the National Academy of Sciences 117, 17084–17093.

Cox, R.T., Van Arsdale, R.B., 2002. The Mississippi Embayment, North America: a first order continental structure generated by the Cretaceous superplume mantle event. Journal of Geodynamics 34, 163–176.

Dastas, N., Chamberlain, J., Garb, M., 2014. Cretaceous–Paleogene dinoflagellate biostratigraphy and the age of the Clayton Formation, Southeastern Missouri, USA. Geosciences 4, 1–29.

Eddy, M.P., Schoene, B., Samperton, K.M., Keller, G., Thierry, A., Khadri, S.F.R., 2020. U-Pb zircon age constraints on the earliest eruptions of the Deccan Large Igneous Province, Malwa Plateau, India. Earth and Planetary Science Letters 540, 1–8.

Edwards, L.E., Gohn, G.S., Self-Trail, J.M., Prowell, D.C., Bybell, L.M., Bardot, L.P., Firth, J.V., Huber, B.T., Frederiksen, N.O., MacLeod, K.G., 1999. Physical Stratigraphy, Paleontology, and Magnetostratigraphy of the USGS - Santee Coastal Reserve Core (CHN-803), Charleston County, South Carolina. Open-File Report 00-308. U.S. Department of the Interior., U.S. Geological Survey.

Firth, John V., 1987. Dinoflagellate biostratigraphy of the Maastrichtian to Danian interval in the U.S. geological servey Albany core, Georgia, U.S.A. Palynology 11, 199–216.

FitzPatrick, M.E.J., Forber, D.A., Hart, M.B., 2018. Dinocyst stratigraphy and paleoenvironmental interpretation of the Cretaceous–Paleogene boundary at Stevns Klint, Denmark. Cretaceous Research 87, 408–442.

Friedrich, O., 2005. Climatic changes in the late Campanian–early Maastrichtian: micropaleontological and stable isotopic evidence from an epicontinental sea. The Journal of Foraminiferal Research 35, 228–247.

Gardin, S., 2002. Late Maastrichtian to early Danian calcareous nannofossils at Elles (Northwest Tunisia). A tale of one million years across the K–T boundary. Palaeogeography, Palaeoclimatology, Palaeoecology 178, 211–231.

Gardin, S., Galbrun, B., Thibault, N., Coccioni, R., Silva, I.P., 2012. Bio-magnetochronology for the upper Campanian–Maastrichtian from the Gubbio area, Italy: new results from the Contessa Highway and Bottaccione sections. Newsletters on Stratigraphy 45, 75–103.

Gilleaudeau, G.J., Voegelin, A.R., Thibault, N., Moreau, J., Ullmann, C.V., Klaebe, R.M., Korte, C., Frei, R., 2018. Stable isotope records across the Cretaceous–Paleogene transition, Stevns Klint, Denmark: new insights from the chromium isotope system. Geochimica et Cosmochimica Acta 235, 305–332.

Hart, M.B., Leighton, A.D., Smart, C.W., Pettit, L.R., Medina-Sanchez, I.N., Harries, P.J., Cardenas, A.L., Hall-Spencer, J.M., Prol-Ledesma, R.M., 2014. Ocean acidification in modern seas and its recognition in the geological record: the Cretaceous/Paleogene boundary in Texas and Alabama. Gulf Coast Associations of Geological Societies Transactions 64, 193–213.

Henehan, M.J., Ridgwell, A., Thomas, E., Zhang, S., Alegret, L., Schmidt, D.N., Rae, J.W.B., Witts, J.D., Landman, N.H., Greene, S.E., Huber, B.T., Super, J.R., Planavsky, N.J., Hull, P.M., 2019. Rapid ocean acidification and protracted Earth system recovery followed the end-Cretaceous Chicxulub impact. Proceedings of the National Academy of Sciences 116, 22500–22504.

Huck, S., Wohlwend, S., Coimbra, R., Christ, N., Weissert, H., 2017. Disentangling shallow-water bulk carbonate carbon isotope archives with evidence for multi-stage diagenesis: an in-depth component-specific petrographic and geochemical study from Oman (mid-Cretaceous). The Depositional Record 3, 233–257.

Hull, P.M., Bornemann, A., Penman, D.E., Henehan, M.J., Norris, R.D., Wilson, P.A., Blum, P., Alegret, L., Batenburg, S.J., Bown, P.R., Bralower, T.J., Cournede, C., Deutsch, A., Donner, B., Friedrich, O., Jehle, S., Kim, H., Kroon, D., Lippert, P.C., ... Zachos, J.C., 2020. On impact and volcanism across the Cretaceous–Paleogene boundary. Science 367, 266–272.

Huybers, P., Aharonson, O., 2010. Orbital tuning, eccentricity, and the frequency modulation of climatic precession: FM TO AM. Paleoceanography 25, 4428.

Jarvis, I., Trabucho-Alexandre, J., Gröcke, D.R., Uličný, D., Laurin, J., 2015. Intercontinental correlation of organic carbon and carbonate stable isotope records: evidence of climate and sea-level change during the Turonian (Cretaceous). The Depositional Record 1, 53–90.

Keller, G., 2005. Biotic effects of late Maastrichtian mantle plume volcanism: implications for impacts and mass extinctions. Lithos 79, 317–341.

Keller, G., Mateo, P., Monkenbusch, J., Thibault, N., Punekar, J., Spangenberg, J.E., Abramovich, S., Ashckenazi-Polivoda, S., Schoene, B., Eddy, M.P., Samperton, K.M., Khadri, S.F.R., Adatte, T., 2020. Mercury linked to Deccan Traps volcanism, climate change and the end-Cretaceous mass extinction. Global and Planetary Change 194, 103312.

Kodama, K.P., Hinnov, L.A., 2015. Rock Magnetic Cyclostratigraphy. Wiley-Blackwell, West Sussex, UK, p. 176.

Landman, N.H., Johnson, R.O., Edwards, L.E., 2004. Cephalopods from the Cretaceous/Tertiary boundary interval on the Atlantic Coastal Plain, with a description of the highest ammonite zones in North America, part 2. Northeastern Monmouth county, New Jersey. Bulletin of the American Museum of Natural History 287, 1–107.

Landman, N.H., Johnson, R.O., Garb, M.P., Edwards, L.E., Kyte, F.T., 2007. Cephalopods from the Cretaceous/Tertiary boundary interval on the Atlantic Coastal Plain, with a description of the highest ammonite zones in North America. Part III. Manasquan River Basin Monmouth County, New Jersey. Bulletin of the American Museum of Natural History 303, 1–122.

Larina, E., Garb, M., Landman, N., Dastas, N., Thibault, N., Edwards, L., Phillips, G., Rovelli, R., Myers, C., Naujokaityte, J., 2016. Upper Maastrichtian ammonite biostratigraphy of the Gulf Coastal Plain (Mississippi Embayment, southern USA). Cretaceous Research 60, 128–151.

Laskar, J., Robutel, P., Joutel, F., Gastineau, M., Correia, A.C.M., Levrard, B., 2004. A long-term numerical solution for the insolation quantities of the Earth. Astronomy & Astrophysics 428, 261–285.

Laskar, J., Fienga, A., Gastineau, M., Manche, H., 2011. La2010: a new orbital solution for the long-term motion of the Earth. Astronomy and Astrophysics 532, 1–15.

Li, M., Hinnov, L., Kump, L., 2019. Acycle: time-series analysis software for paleoclimate research and education. Computers & Geosciences 127, 12–22.

Liu, K., 2009. Oxygen and carbon isotope analysis of the Mooreville Chalk and late Santonian-early Campanian sea level and sea surface temperature changes, northeastern Gulf of Mexico, U.S.A. Cretaceous Research 30, 980–990.

Lottaroli, F., Catrullo, D., 2000. The calcareous nannofossil biostratigraphic framework of the Late Maastrichtian–Danian North Sea chalk. Marine Micropaleontology 39, 239–263.

Mancini, E., 1996. Integrated biostratigraphic and sequence stratigraphic framework for Upper Cretaceous strata of the eastern Gulf Coastal Plain, USA. Cretaceous Research 17, 645–669.

Mancini, E.A., Tew, B.H., Smith, C.C., 1989. Cretaceous–Tertiary contact, Mississippi and Alabama. The Journal of Foraminiferal Research 19, 93–104.

Mann, M.E., Lees, J.M., 1996. Robust estimation of background noise and signal detection in climatic time series. Climatic Change 33, 409–445.

Meyers, S.R., 2015. The evaluation of eccentricity-related amplitude modulation and bundling in paleoclimate data: an inverse approach for astrochronologic testing and time scale optimization: astrochronologic testing and optimization. Paleoceanography 30, 1625–1640.

Mitchell, S.F., Ball, J.D., Crowley, S.F., Marshall, J.D., Paul, C.R.C., Veltkamp, C.J., Samir, A., 1997. Isotope data from Cretaceous chalks and foraminifera: environmental of diagenetic signals? Geology 25, 691–694.

Nifuku, K., Kodama, K., Shigeta, Y., Naruse, H., 2009. Faunal turnover at the end of the Cretaceous in the North Pacific region: implications from combined magnetostratigraphy and biostratigraphy of the Maastrichtian Senpohshi Formation in the eastern Hokkaido Island, northern Japan. Palaeogeography, Palaeoclimatology, Palaeoecology 271, 84–95.

Pospichal, J.J., Wise Jr., S.W., 1990. Calcareous nannofossils across the K–T boundary, ODP Hole 690C, Maud Rise, Weddell Sea. Proceeding of the Ocean Drilling Program, Scientific Results 113, 515–532.

Pryor, W.A., 1960. Cretaceous sedimentation in the Upper Mississippi embayment. Bulletin of the American Association of Petroleum Geologists 44, 1473–1504.

Puckett, M.T., 2005. Santonian–Maastrichtian planktonic foraminiferal and ostracod biostratigraphy of the Northern Gulf Coastal Plain, USA. Stratigraphy 2, 117–146.

Punekar, J., Keller, G., Khozyem, H.M., Adatte, T., Font, E., Spangenberg, J., 2016. A multi-proxy approach to decode the end-Cretaceous mass extinction. Palaeogeography, Palaeoclimatology, Palaeoecology 441, 116–136.

Razmjooei, M.J., Thibault, N., Kani, A., Dinarès-Turrell, J., 2020. Calcareous nannofossil response to Late Cretaceous climate change in the eastern Tethys (Zagros Basin, Iran). Palaeogeography, Palaeoclimatology, Palaeoecology 538, 109418.

Saunders, A.D., 2005. Large igneous provinces: origin and environmental consequences. Elements 1, 259–263.

Schettino, A., Scotese, C.R., 2005. Apparent polar wander paths for the major continents (200 Ma–Present Day): a paleomagnetic reference frame for global plate tectonic reconstructions. Geophysical Journal International 163, 727–759.

Schoene, B., Eddy, M.P., Samperton, K.M., Keller, C.B., Keller, G., Adatte, T., Khadri, S.F.R., 2019. U–Pb constraints on pulsed eruption of the Deccan Traps across the end-Cretaceous mass extinction. Science 363, 862–866.

Schulte, P., Alegret, L., Arenillas, I., Arz, J.A., Barton, P.J., Bown, P.R., Bralower, T.J., Christeson, G.L., Claeys, P., Cockell, C.S., Collins, G.S., Deutsch, A., Goldin, T.J., Goto, K., Grajales-Nishimura, J.M., Grieve, R.A.F., Gulick, S.P.S., Johnson, K.R., Kiessling, W., ... Willumsen, P.S., 2010. The Chicxulub asteroid impact and mass extinction at the Cretaceous–Paleogene boundary. Science 327, 1214–1218.

Sheehan, P.M., Hansen, T.A., 1986. Detritus feeding as a buffer to extinction at the end of the Cretaceous. Geology 14, 868–870.

Sheldon, E., Ineson, J., Bown, P., 2010. Late Maastrichtian warming in the Boreal Realm: Calcareous nannofossil evidence from Denmark. Palaeogeography, Palaeoclimatology, Palaeoecology 295, 55–75.

Sinnesael, M., De Vleeschouwer, D., Coccioni, R., Claeys, P., Frontalini, F., Jovane, L., Savian, J.F., Montanari, A., 2016. High-resolution multiproxy cyclostratigraphic analysis of environmental and climatic events across the Cretaceous–Paleogene boundary in the classic pelagic succession of Gubbio (Italy). Geological Society of America, Special Paper vol. 524.

Sinnesael, M., de Winter, N.J., Snoeck, C., Montanari, A., Claeys, P., 2018. An integrated pelagic carbonate multi-proxy study using portable X-ray fluorescence (pXRF): Maastrichtian strata from the Bottaccione Gorge, Gubbio, Italy. Cretaceous Research 91, 20–32.

Sinnesael, M., Montanari, A., Frontalini, F., Coccioni, R., Gattacceca, J., Snoeck, C., Wegner, W., Koeberl, C., Morgan, L.E., de Winter, N.J., DePaolo, D.J., Claeys, P., 2019. Multiproxy Cretaceous–Paleogene boundary event stratigraphy: an Umbria–Marche basinwide perspective. 250 Million Years of Earth History in Central Italy: Celebrating 25 Years of the Geological Observatory of Coldigioco vol 542.

Smit, J., Roep, T.B., Alvarez, W., Montanari, A., Claeys, P., Grajales-Nishimura, J.M., Bermudez, J., 1996. Coarse-grained, clastic sandstone complex at the K/T boundary around the Gulf of Mexico: deposition by tsunami waves induced by the Chicxulub impact? In: Ryder, G., Fastovsky, D.E., Gartner, S. (Eds.), The Cretaceous–Tertiary Event and Other Catastrophes in Earth History. vol. 307. Geological Society of America, pp. 151–182

Sprain, C.J., Renne, P.R., Clemens, W.A., Wilson, G.P., 2018. Calibration of chron C29r: new high-precision geochronologic and paleomagnetic constraints from the Hell Creek region, Montana. GSA Bulletin 130, 1615–1644.

Sprain, C.J., Renne, P.R., Vanderkluysen, L., Pande, K., Self, S., Mittal, T., 2019. The eruptive tempo of Deccan volcanism in relation to the Cretaceous–Paleogene boundary. Science 363, 866–870.

Strasser, A.H., Heckel, P.H., 2007. Cyclostratigraphy concepts, definitions, and applications. Newsletters on Stratigraphy 42, 75–114.

Tegner, C., Marzoli, A., McDonald, I., Youbi, N., Lindström, S., 2020. Platinum-group elements link the end-Triassic mass extinction and the Central Atlantic Magmatic Province. Scientific Reports 10, 3482.

Thibault, N., Gardin, S., 2006. Maastrichtian calcareous nannofossil biostratigraphy and paleoecology in the Equatorial Atlantic (Demerara Rise, ODP Leg 207 Hole 1258A). Revue de Micropaleontologie 49, 199–214.

Thibault, N., Gardin, S., 2007. The late Maastrichtian nannofossil record of climate change in the South Atlantic DSDP Hole 525A. Marine Micropaleontology 65, 163–184.

Thibault, N., Gardin, S., 2010. The calcareous nannofossil response to the end-Cretaceous warm event in the Tropical Pacific. Palaeogeography, Palaeoclimatology, Palaeoecology 291, 239–252.

Thibault, N., Husson, D., 2016. Climatic fluctuations and sea-surface water circulation patterns at the end of the Cretaceous era: calcareous nannofossil evidence. Palaeogeography, Palaeoclimatology, Palaeoecology 441, 152–164.

Thibault, N., Husson, D., Harlou, R., Gardin, S., Galbrun, B., Huret, E., Minoletti, F., 2012. Astronomical calibration of upper Campanian–Maastrichtian carbon isotope events and calcareous plankton biostratigraphy in the Indian Ocean (ODP Hole 762C): implication for the age of the Campanian–Maastrichtian boundary. Palaeogeography, Palaeoclimatology, Palaeoecology 337–338, 52–71.

Thibault, N., Galbrun, B., Gardin, S., Minoletti, F., Le Callonnec, L., 2016a. The end-Cretaceous in the southwestern Tethys (Elles, Tunisia): orbital calibration of paleoenvironmental events before the mass extinction. International Journal of Earth Sciences 105, 771–795.

Thibault, N., Harlou, R., Schovsbo, N.H., Stemmerik, L., Surlyk, F., 2016b. Late Cretaceous (late Campanian–Maastrichtian) sea-surface temperature record of the Boreal Chalk Sea. Climate of the Past 12, 429–438.

Thomson, D.J., 1982. Spectrum estimation and harmonic analysis. Proceedings of the IEEE 70, 1055–1096.

Vellekoop, J., Sluijs, A., Smit, J., Schouten, S., Weijers, J.W.H., Sinninghe Damste, J.S., Brinkhuis, H., 2014. Rapid short-term cooling following the Chicxulub impact at the Cretaceous–Paleogene boundary. Proceedings of the National Academy of Sciences 111, 7537–7541.

Vellekoop, Johan, Esmeray-Senlet, S., Miller, K.G., Browning, J.V., Sluijs, A., van de Schootbrugge, B., Sinninghe Damsté, J.S., Brinkhuis, H., 2016. Evidence for Cretaceous–Paleogene boundary bolide "impact winter" conditions from New Jersey, USA. Geology 44, 619–622.

Waltham, D., 2015. Milankovitch period uncertainties and their impact on cyclostratigraphy. Journal of Sedimentary Research 85, 990–998.

Watkins, D.K., Self-Trail, J.M., 2005. Calcareous nannofossil evidence for the existence of the Gulf Stream during the late Maastrichtian: Maastrichtian Gulf Stream. Paleoceanography 20, 1–9.

Weedon, G.P., 2003. Time-series Analysis and Cyclostratigraphy: Examining Stratigraphic Records of Environmental Cycles. 1st ed. Cambridge University Press, Cambridge, UK, p. 280.

Westphal, H., Hilgen, F., Munnecke, A., 2010. An assessment of the suitability of individual rhythmic carbonate successions for astrochronological application. Earth-Science Reviews 99, 19–30.

Wignall, P.B., 2001. Large igneous provinces and mass extinctions. Earth-Science Reviews 53, 1–33.

Witts, J.D., Landman, N.H., Garb, M.P., Boas, C., Larina, E., Rovelli, R., Edwards, L.E., Sherrell, R.M., Cochran, J.K., 2018. A fossiliferous spherule-rich bed at the Cretaceous–Paleogene (K–Pg) boundary in Mississippi, USA: implications for the K–Pg mass extinction event in the Mississippi Embayment and Eastern Gulf Coastal Plain. Cretaceous Research 91, 147–167.

Witts, J.D., Landman, N.H., Garb, M.P., Irizarry, K.M., Larina, E., Thibault, N., Razmjooei, M.J., Yancey, T.E., Myers, C.E., 2021. Cephalopods from the Cretaceous–Paleogene (K–Pg) boundary interval on the Brazos River, Texas, and extinction of the ammonites. American Museum Novitates 2020, 3964.

Zachos, J.C., Arthur, M.A., Dean, W.E., 1989. Geochemical and paleoenvironmental variations across the Cretaceous/Tertiary boundary at Braggs, Alabama. Palaeogeography, Palaeoclimatology, Palaeoecology 69, 245–266.